Strål
säkerhets
myndigheten
Swedish Radiation Safety Authority

Authors: Jessica Strömbro
Magnus Dahlberg

Research

2011:04

Evaluation of the Technical Basis for New Proposals of Fatigue Design of Nuclear Components

Report number: 2011:04 ISSN: 2000-0456
Available at www.stralsakerhetsmyndigheten.se

SSM perspective

Background

During the recent years fatigue analysis procedures for nuclear components have been investigated. The most common method so far has been the American code ASME III. The basis for the current design procedures in ASME III is quite old and has now been evaluated against modern data leading to the proposal of modified design curves.

Also the effect of the environment has been the subject of intense study in USA, Japan and elsewhere. Several reports indicate a potentially large influence of the environment, leading to the proposal of entirely new calculation procedures.

The background for the new design curves and the environmental effect procedures are evaluated in this report.

Objectives

The principal objective of the project is to use the latest research results regarding the design of fatigue to evaluate the technical basis for new proposal regarding an update of fatigue curves and the correction for environmental effects.

Results

- Argonne national Laboratory (ANL) in USA has performed a unique review of fatigue data. On basis of this review, ANL has proposed new fatigue design curves for austenitic steels, carbon steels and low-alloy steels. The proposals are based on comprehensive studies of data from several modern databases. The data has been consistently evaluated in this report.
- The ANL design curves are much more consistent with modern data for common austenitic steels, such as SS304/316 than the current ASME III design curves. The current ASME III fatigue design curves for austenitic steels potentially contain smaller margins than previously expected.
- An extensive amount of literature on environmental effects on fatigue has been studied. There is no doubt that LWR environment may significantly decrease the fatigue life in comparison to air environment.
- The environmental effects noticed in recent experiments conducted mainly in Japan and USA were not explicitly included in the current design curves. Hence, there is a concern that the margins in the current ASME fatigue design procedure are smaller than expected.
- Applicable models for incorporating environmental effects in fatigue design calculations have been proposed in USA (ANL) and Japan (JSME). These models seem to incorporate the very complex phenomenon of environmental effects in a reasonable way.

- The controlling parameters in these models are temperature and strain rate, in addition, for carbon and low-alloy steels, the sulphur content in the steel as well as the dissolved oxygen content in the water.
- The decrease in fatigue life is caused primarily during growth of micro-structurally short cracks. Environmental effects decreases as the cracks grow larger (> 200 μm).

Need for further research

The results of this project will be used by SSM in safety assessments of fatigue loaded components. More research is needed for the further investigation of influencing parameters of the fatigue design curves and to find out the real margin in the ASME III fatigue design procedure.

Project information

Contact person SSM: Björn Brickstad
Reference: SSM 2009/4144, 2037028-02
Project organization: Inspecta Technology AB has managed the project with Dr Magnus Dahlberg as the project manager. Dr Jessica Strömbro at Inspecta Nuclear AB has been the principal investigator.
Reference:

Strål
säkerhets
myndigheten
Swedish Radiation Safety Authority

Authors: Jessica Strömbro, Inspecta Nuclear AB, Stockholm, Sweden
Magnus Dahlberg, Inspecta Technology AB, Stockholm, Sweden

2011:04

Evaluation of the Technical Basis for New Proposals of Fatigue Design of Nuclear Components

Date: January 2011
Report number: 2011:04 **ISSN:** 2000-0456
Available at www.stralsakerhetsmyndigheten.se

SSM 2011:04

Table of content *Page*

1 INTRODUCTION

Some parts of the common fatigue analysis procedure for nuclear components (ASME III) have been under investigation in recent years. These investigations have focused mostly on the fatigue design curves and environmental effects. The fatigue design curves are today quite old, and have been evaluated against modern data leading to the proposal of modified design curves.

The effect of the environment has been the subject of intense study in USA, Japan and elsewhere. Several reports indicate a potentially large influence of the environment, leading to the proposal of entirely new calculation procedures.

The background for the new design curves and the environmental effect procedures are evaluated in this report. Some other effects are also discussed. The initially stated scope of the project concerned the following:

- Design curves and their background for austenitic and ferritic steels.
- Environmental effects
- The influence of residual stresses
- Criteria for multi-axial fatigue
- Factors for plastic deformation effects

The scope of the project was somewhat altered during the course of the project. Environmental effects turned out to be of crucial interest. Hence, the study of these effects was increased at the expense of residual stresses, multi-axial effects and plastic deformation. In hindsight this modification seems entirely right, taken the strong interest in the environmental effects from both SSM and the industry. Two interim reports have been previously released in this project, on request by SSM.

2 FATIGUE CURVES

2.1 Current fatigue curves and philosophy

The most widely used design procedure for NPP components is that presented in the ASME Section III Division 1 code [1]. Notably, these curves were established on basis of strain controlled fatigue tests on small specimen in air, the so called Langer experiments. The tests were interrupted by complete failure of the specimen. Mean fatigue curves where derived form the test. Fatigue curves in terms of stresses were obtained by multiplying the total strain with the elastic modulus. The relation between the (fictitious) stress amplitude and number of cycles to failure are formally written as

$$S_a = \frac{B}{N_f^{0.5}} + S_e . \tag{1}$$

The mean curves can hence be expressed by the different values of B and S_e. In (1), S_a represents stress amplitude and N_f represents the number of cycles to failure.

Table 1 Mean curve Langer data. Parameters B and S_e for Eq. (1).

Material type	B (GPa)	S_e (MPa)
Carbon steel	59.734	149.2
Low-alloy steel	49.222	265.4
Austenitic steel SS	58.020	299.9

In ASME III [1], the design fatigue curves have been obtained from the laboratory tests by reducing the fatigue life at each point on the curve by a factor of 2 on strain (or stress) or 20 on cycles, whichever is the more conservative. Cooper [2] noted that the intent of introducing these factors was to account for such factors as data scatter (including material variability), differences in surface condition and size differences between the test specimens and the actual components. Cooper further noted that the factors of 2 and 20 were not safety margins but rather uncertainty factors or *transferability factors* that should be applied to the small–specimen data to obtain reasonable estimates of the lives of actual reactor components. He believed that the factor 20 was made up from the product of the following three uncertainties:

- Material variability and scatter on data between the minimum and mean, 2.0
- Size effects (difference in scale between laboratory samples and plant), 2.5
- Surface finish, atmosphere (moderate environmental effects), metallurgy, etc. 4.0

However, whatever the historical origin of the safety factors in the ASME design codes, the fatigue design curves have been adopted in both the French RCC-M and German KTA codes and so are widely used around Europe.

Initially, the design curves where intended for lives with $N < 10^6$. The design curve for austenitic steels where later on extended for longer lives. This design curve included no mean stress correction, unlike the other curves. A greater need to correct for mean stress in the high cycle regime even for austenitic steels was identified. The effects of mean stress were possibly taken into account using a correction according to the empirical Goodman correction[1], which involves ultimate strength, yield strength and mean stress.

The design curves are shown in the below, Figure 1, Figure 2 and Figure 3. Figure 3 shows that there are three options; A, B and C, for austentic steels for $N > 10^6$. The somewhat un-clear criteria for

choosing either curve A, B or C are shown in Figure 3. In fact, curves B and C are adopted to match the Jaske curves[4] depicted in Figure 10. The Curve B then corresponds to Jaske's data without mean stress correction, whereas curve C corresponds to Jaske's data corrected for maximum mean tensile stress by a Goodman correction.

FIG. I-9.1M DESIGN FATIGUE CURVES FOR CARBON, LOW ALLOY, AND HIGH TENSILE STEELS FOR METAL TEMPERATURES NOT EXCEEDING 370°C

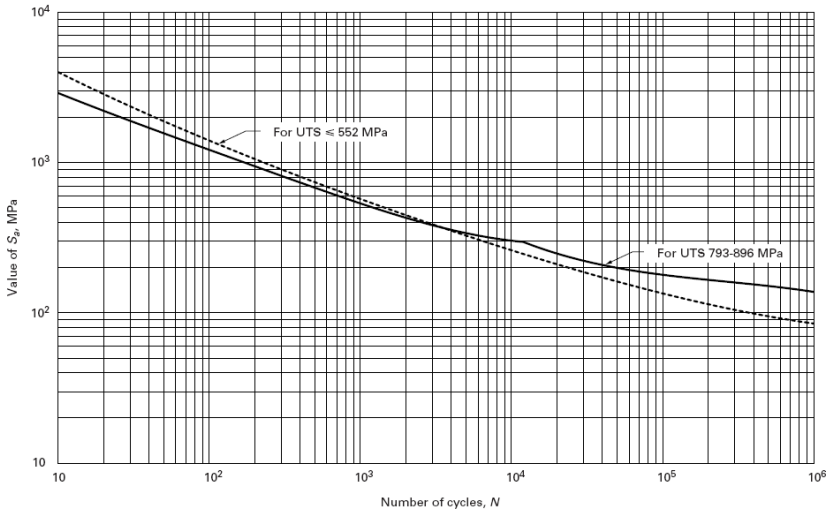

Figure 1. ASME fatigue curves for carbon steels, low-alloy steels etc.

FIG. I-9.2.1M DESIGN FATIGUE CURVES FOR AUSTENITIC STEELS, NICKEL–CHROMIUM–IRON ALLOY, NICKEL–IRON–CHROMIUM ALLOY, AND NICKEL–COPPER ALLOY FOR S_a > 194 MPa FOR TEMPERATURES NOT EXCEEDING 425°C

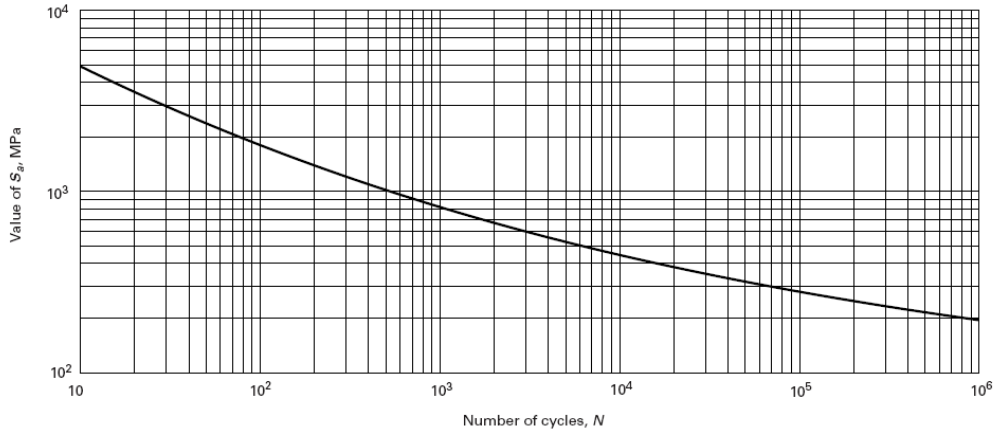

Figure 2. ASME fatigue curve for austenitic steels etc. Valid for $N < 10^6$.

FIG. I-9.2.2M DESIGN FATIGUE CURVES FOR AUSTENITIC STEELS, NICKEL–CHROMIUM–IRON ALLOY, NICKEL–IRON–CHROMIUM ALLOY, AND NICKEL–COPPER ALLOY FOR $S_a \leq 194$ MPa FOR TEMPERATURES NOT EXCEEDING 425°C

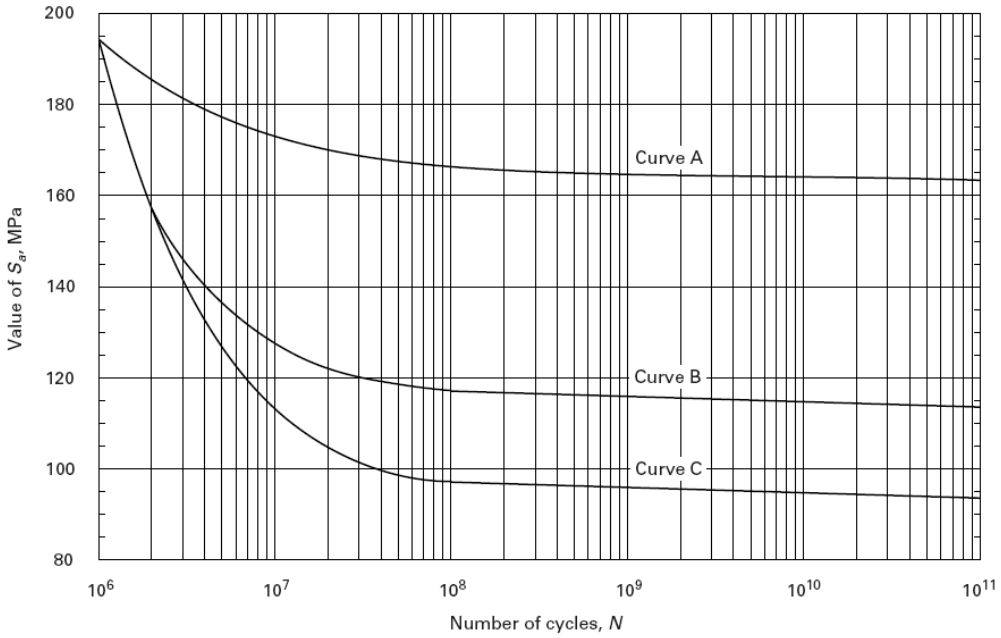

Criteria for the Use of the Curves in Figs. I-9.2.2 and I-9.2.2M

Curve	Elastic Analysis of Material Other Than Welds and Adjacent Base Metal	Elastic Analysis of Welds and Adjacent Base Metal
A	$(P_L + P_b + Q)_{Range} \leq 27.2$ ksi (188 MPa)	...
B	$(P_L + P_b + Q)_{Range} > 27.2$ ksi (188 MPa) and S_a is corrected for applied mean stress	$(P_L + P_b + Q)_{Range} \leq 27.2$ ksi (188 MPa)
C	$(P_L + P_b + Q)_{Range} > 27.2$ ksi (188 MPa)	$(P_L + P_b + Q)_{Range} > 27.2$ ksi (188 MPa)

GENERAL NOTES:
(a) Range applies to the individual quantities P_L, P_b, and Q and applies to the set of cycles under consideration.
(b) Thermal bending stresses resulting from axial and radial gradients are excluded from Q.
(c) Curve A is also to be used with inelastic analysis with $S_a = \frac{1}{2} \Delta e_t E$, where Δe_t is the total effective strain range.
(d) The maximum effect of retained mean stress is included in Curve C.
(e) The adjacent base metal is defined as three wall thicknesses from the center line of the weld.

Figure 3. ASME fatigue curve for austenitic steels etc. Valid for N > $10^{6.}$ Choice of curve A, B and C is based on configuration and on the level of mean stress, stress range and presence of weld, as described in the figure.

2.2 Review of the fatigue data according to ANL in NUREG/CR-6909

Alongside the study of environmental effects, an extensive review of the fatigue curves where carried out by ANL in NUREG/CR-6909 [3]. There had been previous concern about the fatigue curves for austenitic steels already in the 70's. A major study was preformed by Jaske and O'Donnel [4], where some potential non-conservatism of the original fatigue curves for austenitic steels was identified. The new experiments gave mean curves that deviated from the Langer curves. This deviation has been confirmed in several other studies. ANL studied large sets of data from several different sources. Mean curves where established on the form

$$\ln(N) = A - B\ln(\varepsilon_a - C). \quad (2)$$

Here, ε_a is the strain amplitude and N is the number of cycles to failure. This equation provides the basis for the ANL model. The parameters *A*, *B* and *C* in (2) are constants to be determined. *C* represents the fatigue limit, *B* represents the exponent and *A* basically represents the low-cycle fatigue behavior. By adopting these parameters to the fatigue data, ANL-models were obtained for the different material types. An extensive analysis on the parameters controlling the fatigue life of components was also made. Such parameters are size effects, surface roughness effects, mean stress effects, loading history effects and material scatter. The interruption criterion in modern tests is somewhat different in modern experiments, than those used by Langer. A drop in tensile stress of 25% (corresponding to a certain drop of stiffness, since the experiment is in strain control) is used as criterion. Most specimens are cylindrical with a size of 5-10 mm. The drop of 25% corresponds approximately to a crack of size 3 mm deep.

New design curves are proposed on basis of the ANL-models, see Figures 4 and 5. The investigation showed that the code mean curves for non-austenitic steels all are adequate, in line with the proposed ANL-curves, or even somewhat conservative. The mean curves were derived in room temperature. The fatigue lives are shortened for higher temperatures, but should be well covered within the transferability factors.

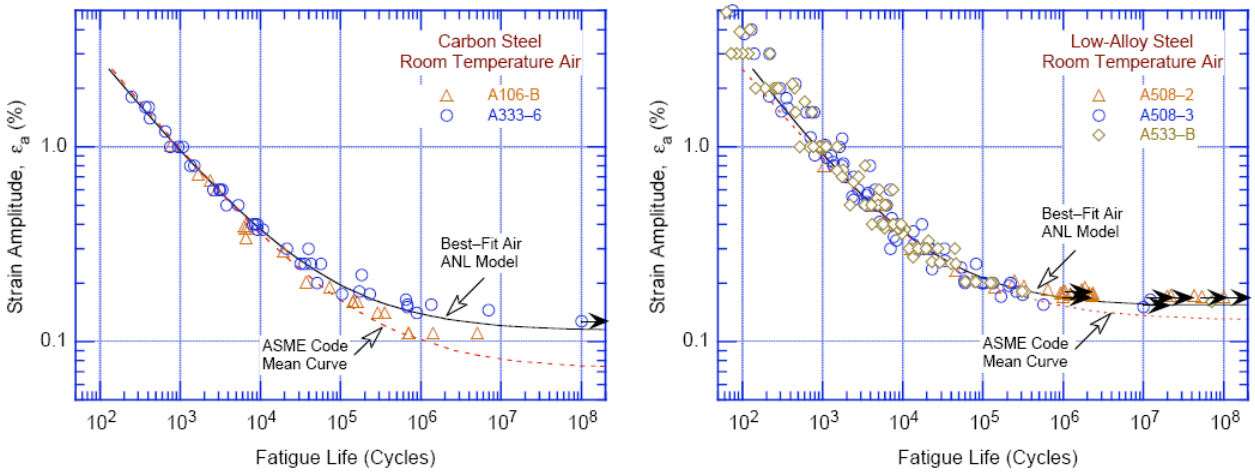

Figure 4. Data for carbon steel and low-alloy steel in room temperature. The ASME Code mean curve and the ANL-curve are in agreement.

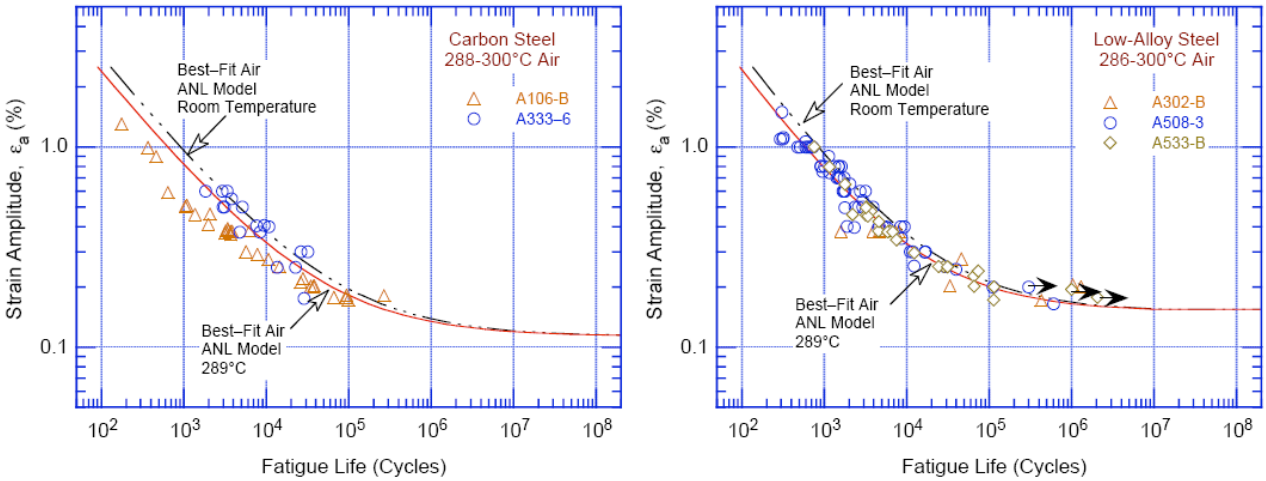

Figure 5. Data for carbon steel and low-alloy steel in high temperature. The influence of high temperature, up to 300°C, is included in the transferability factors.

The situation for austenitic steels is more problematic. The ANL investigation of experiments in air confirmed that the Langer mean curve is consistently higher than most data collected over the past 30 years. This discrepancy concerns data for N > 10^4. This is readily shown in Figure 6 below. This discrepancy is not new, and has been demonstrated in earlier studies, see for example Figure 7.

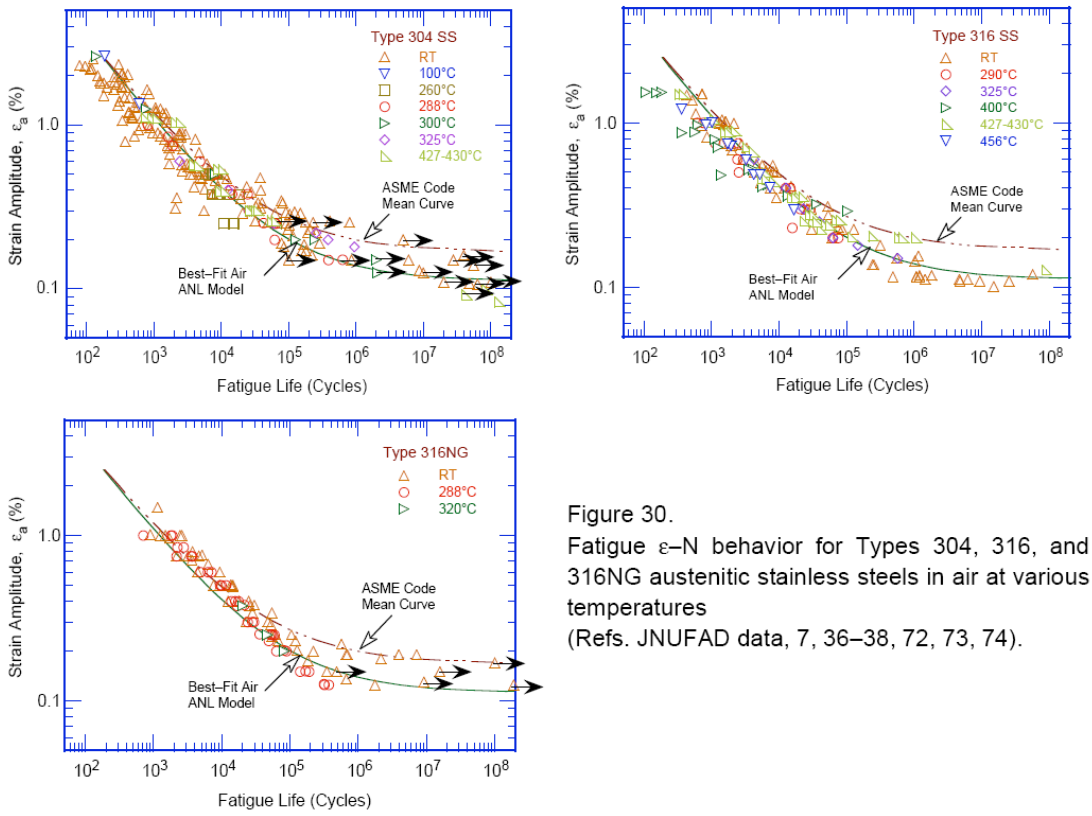

Figure 30.
Fatigue ε–N behavior for Types 304, 316, and 316NG austenitic stainless steels in air at various temperatures
(Refs. JNUFAD data, 7, 36–38, 72, 73, 74).

Figure 6. Data for three types of austenitic steel, 304, 316 and 316NG.

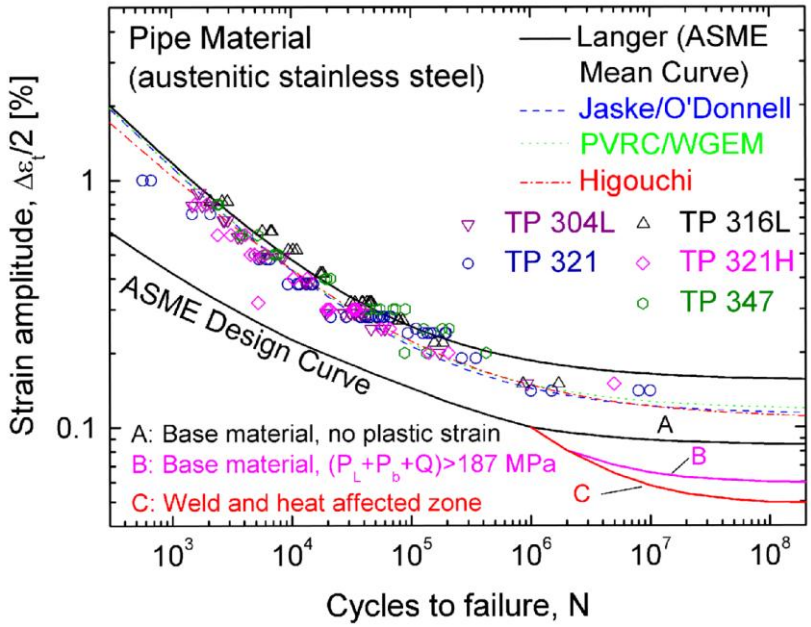

Figure 7. Comparison of data with the ASME design curve for stainless steel.

Fatigue data for Ni-Cr-Fe alloys and corresponding weld materials (for example Alloy 600 and weld material Alloy182) are also discussed in NUREG/CR-6909 [3]. The data are consistent with the ANL proposal for austenitic materials. Hence, the ANL design curve for austenitic materials applies for these materials as well.

2.3 Review of the margins of the ASME fatigue design curves according to ANL

The NUREG/CR-6909 report also included a thorough review of the transferability factors of 2 on strain (or stress) or 20 on cycles. The analysis is performed by reconsidering the influence of the parameters, Data scatter and material variability, size effects and surface factors. These were the factors that had been previously considered by Cooper for the current ASME fatigue curves. Additionally, ANL considered the effect of loading history. It is well known that the order of higher and lower loads in a spectrum may affect the fatigue life. The comparison was made carefully for lives within the low-cycle regime. The existing database was employed for the study.

Table 2. Factors on life (transferability factors) to account for various effects between specimen and component.

Parameter	*ASME (Cooper)*	*ANL Study*
Material variability and Data Scatter (minimum to mean)	2	2.1-28
Size effects	2.5	1.2-1.4
Surface finish, moderate environmental effects, metallurgy, etc	4	2.0-3.5
Loading history	-	1.2-2
Total Adjustment	20	6.0-27.4

As shown in the above table the variation in the factors can be relatively large. In order to estimate the most appropriate values, statistical distribution were attempted for each parameter. This allowed for (numerical) statistical calculation of the total adjustment. The calculations were carried out by Monte-

Carlo simulations, with the statistical distribution of each factor as input. The computations lead to an estimate of the modification of the fatigue life of the specimens to a component that is hypothetically affected the parameters in Table 2. The results are expressed in terms of the parameter *A* in Eq. (2), i. e. the parameter that primarily controls the low-cycle fatigue life. The condition set up for the factor on life was that the total adjustment should bound the life of 95% of the component population. The calculations were performed for each material type. The results are shown below in Figure 8.

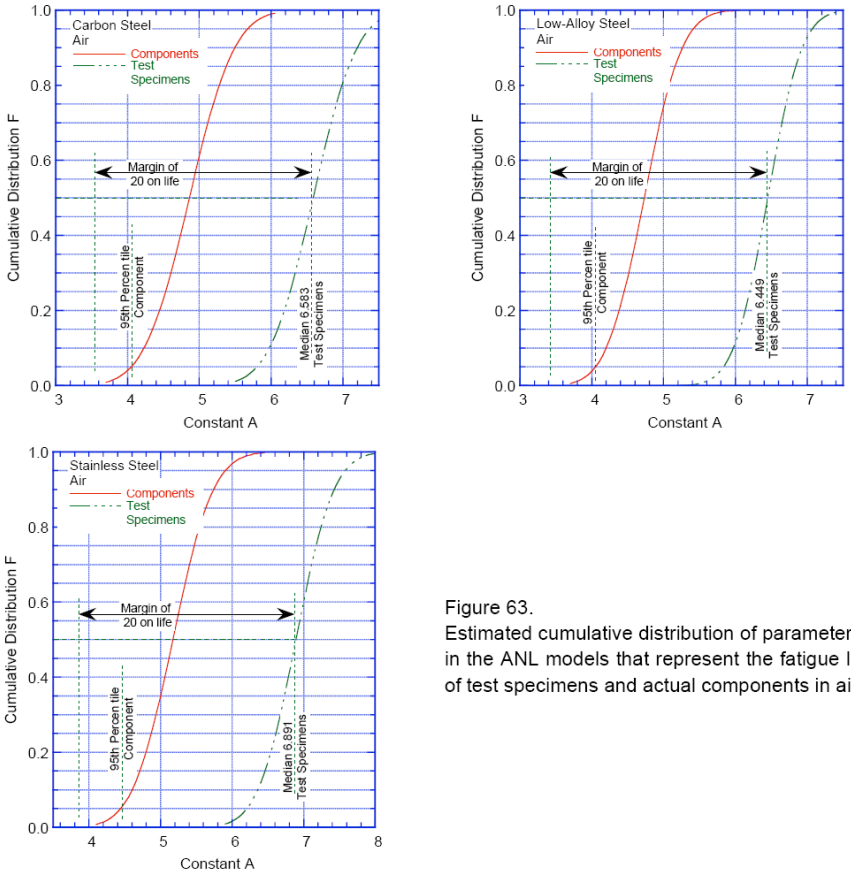

Figure 63.
Estimated cumulative distribution of parameter A in the ANL models that represent the fatigue life of test specimens and actual components in air.

Figure 8. Distribution of the parameter A the ANL-model, for specimens and components in air.

By these calculations, the factor on life (or margin on life) can be estimated for all material types. In fact, the results were quite similar for all material types. The results are comprised in the below Table 3. The results have lead to the suggestions that the new design curves should have a safety factor of 12 instead of 20 on life. Note from that a factor of 20 instead of 12 would lead to a very low probability of failure. See chapter 2.5.2 for a further discussion on margins in design curves.

Table 3. The margin on life in order to bound the fatigue life of 95% of the component population.

Material	*Computed Margin on life*
Carbon steel	12.6
Low-alloy steel	11.0
Austenitic steel SS	11.6

2.4 ANL proposed design curves in air

On basis on the investigation of fatigue data and margins of life new design curves were proposed. The strategy for the fatigue curves can be summarized as follows. The mean fatigue curves are determined by adjusting the ANL-model ($\ln(N) = A - B\ln(\varepsilon_a - C)$, Eq. (2), to the strain-life data in the database. The parameters *A, B* and *C* for the mean curves are shown in the table below.

Table 4. Mean curve ANL data. (Applies for strains in per cent)

Material type	*A*	*B*	*C*
Carbon steel	6.583	1.975	0.113
Low-alloy steel	6.449	1.808	0.151
Austenitic steel SS	6.891	1.920	0.112

In order to establish the design curves the mean curves are first divided by the factor 12 on life or the factor 2 on strain/stress whichever is the most conservative. Thereafter the curves are corrected for the potential presence of a tensile mean stress, by a version of the Goodman relation, assuming fully developed tensile mean stress. The adjusted allowable stress amplitude, $\sigma_{a,\mathrm{adj}}$, is obtained by $\sigma_{a,\mathrm{adj}} = \sigma_a \cdot \left(\left(1-\sigma_y/\sigma_b\right)/\left(1-\sigma_a/\sigma_b\right)\right)$ for $\sigma_a < \sigma_y, \sigma_{a,\mathrm{adj}} = \sigma_a$ for $\sigma_a \geq \sigma_y$, with σ_a denoting the non-adjusted stress amplitude, σ_y the yield stress, and σ_b denoting the ultimate strength.

For non-austenitic steels the ANL curves are less conservative than the ASME design curve, see Figure 9.The situation is the opposite for the austenitic materials. Here, the ANL design curve is more conservative. The difference between ASME and ANL is considerable in the high cycle regime, especially in comparison with the ASME design curve A. In Figure 10, the ANL curves are compared with the ASME curves. Additionally, the Jaske [4] proposed design curves are shown as well. Jaske provided curves based on the option of zero or maximum compensation for tensile mean stresses. It is noted that the Jaske curve corrected for mean stress and the ANL curve is in very good agreement, despite the fact that Jaske uses the factor 20 on life and ANL the factor 12. For lives $N < 10^4$ the difference between all curves is rather limited.

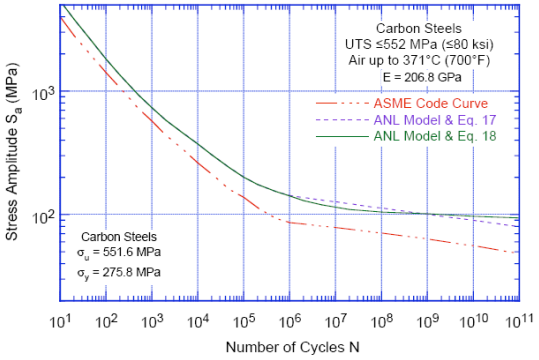

Figure 9.
Fatigue design curve for carbon steels in air. The curve developed from the ANL model is based on factors of 12 on life and 2 on stress.

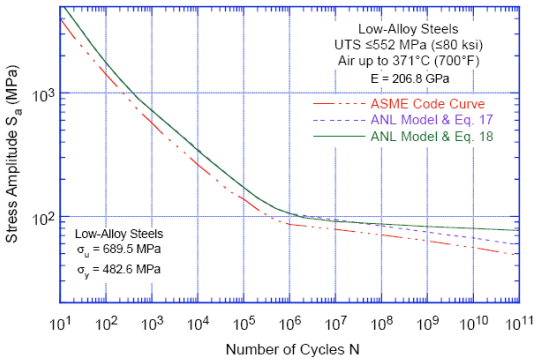

Figure 10.
Fatigue design curve for low-alloy steels in air. The curve developed from the ANL model is based on factors of 12 on life and 2 on stress.

Figure 9. Comparison between the ANL design curves and the current ASME design curves for the non-austenitic material. The ANL design curves are denoted ANL model & Eq. 17 and 18 (which indicate the method for mean stress affects).

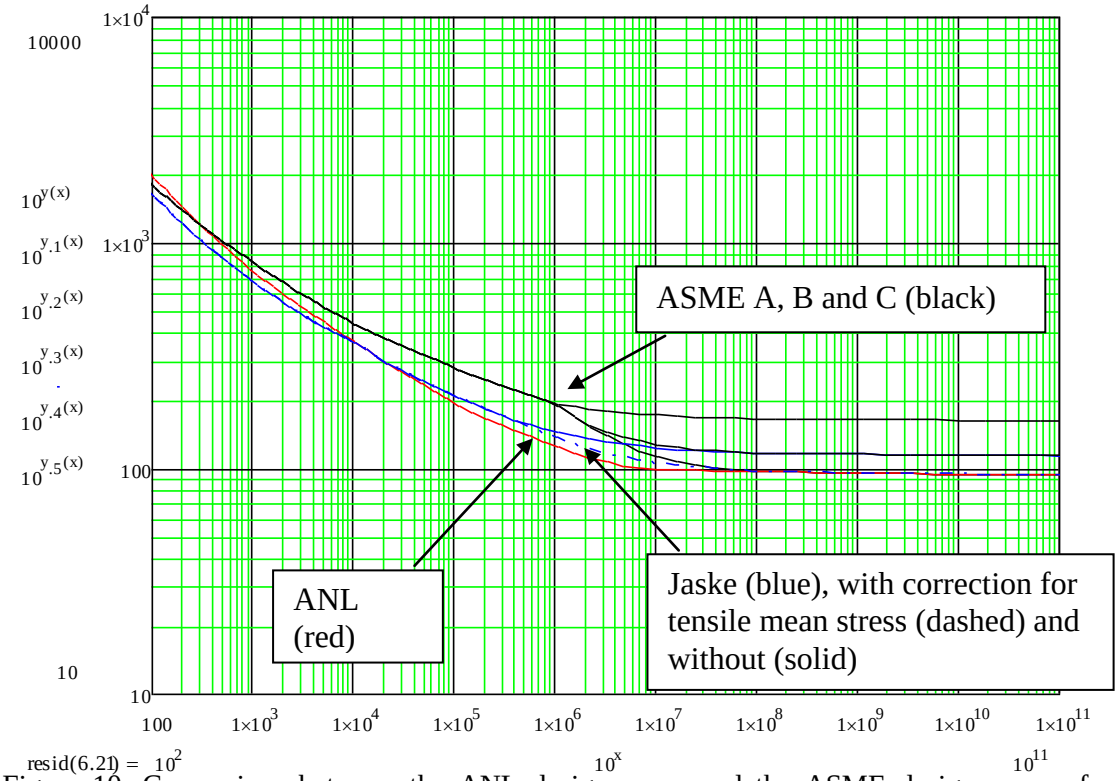

Figure 10. Comparison between the ANL design curve and the ASME design curves for austenitic steels.

2.5 Discussion on the Fatigue curves in air

2.5.1 General Philosophy

Central in the fatigue design philosophy of ASME[1] is that the design curves are derived from strain controlled experiments on small, non-notched specimen in laboratory environment. Since the fatigue curves where derived by strain control, all comparison between computed strains and fatigue curve should be based on strains. In classical design situations however, stresses are computed by an elastic analysis. The stresses are then corrected for stress raisers and possible plastic effects, for example as guided by ASME III NB3200 for design by analysis or NB 3600 for design of piping. Thus an indirect comparison of strains is performed. This works well for components subjected to a load primarily in deformation control, which is the case for thermal loads which is a prime concern for NPP components. As soon as a portion of the total strains is plastic, the stress amplitudes in Eq. (1) will be fictitious and deviate substantially from the real stress. This is important especially for austenitic steels with considerable plastic deformation even near the fatigue limit. This is exemplified by the below figure were the real stresses are computed by the stress-strain relation for SS316 proposed by van Eeten [5]. The strain amplitudes are converted to the real stress amplitudes instead of the fictitious stresses which are obtained by multiplying with the elastic modulus, *E*. The real stresses are compared to the fictitious stresses and a significant difference is observed even in the high cycle regime.

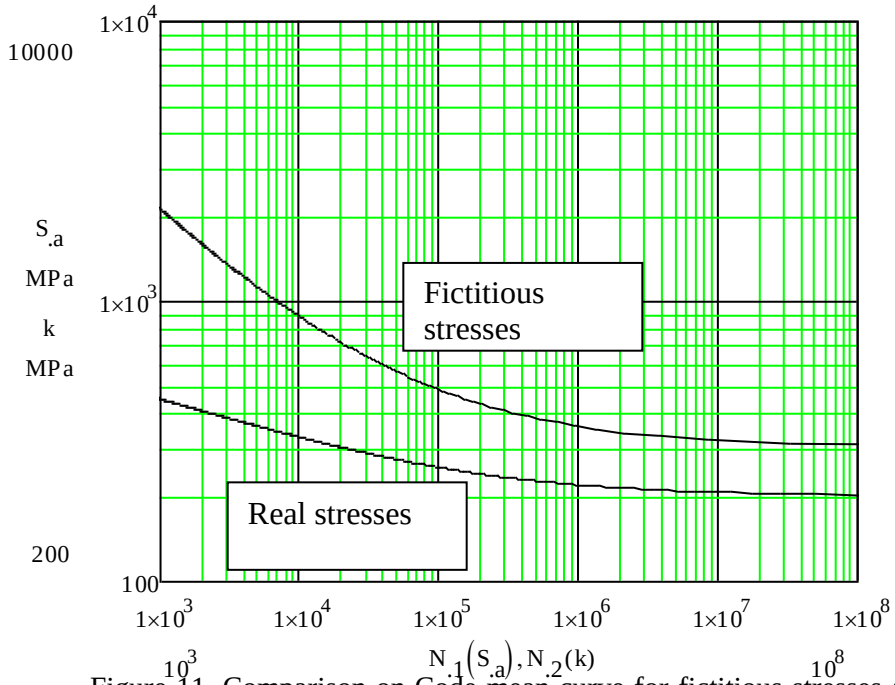

Figure 11. Comparison on Code mean curve for fictitious stresses an l real stresses for an SS 304/316 type austenitic steel.

The use of machined, smooth small specimen also has implication for the applicability of the fatigue design procedure. The fatigue process may be different than that in real component where the fatigue strength may be governed by inherent defects or other defects that may arise during operation. Fatigue life has conventionally been divided into two stages: initiation and crack propagation. This distinction has no clear definition. For a smooth surface initial crack nucleate and propagate in the maximum shear direction. During this stage, stage I, the cracks interact strongly with the microstructure of the material. The cracks are called micro-structurally short cracks. These cracks may grow rapidly in the beginning but be retarded in the interaction with for example grain boundaries. Thereafter the cracks then propagate as mechanically short cracks, stage II. These cracks are much more insensitive to the

microstructure and may continue to grow. Cracks in stage II may for example be analyzed with fracture mechanics (even though there are some limitations).

For many components the presence of cracks will mean that the fatigue process may start well within stage II or even larger cracks. During its fatigue life the component may never encompass nucleation and stage I, which may have been a major part of the fatigue life of the specimen. Materials that are resistant to crack initiation may be much more sensitive to crack propagation. A typical example is high strength steel that in comparison gives high fatigue limits for smooth specimen, but where the fatigue properties may rapidly decrease with the presence of defects and cracks. The ranking of fatigues strength may however be altered once there is a presence of defects and sharp stress raisers. This immediately makes the question of transferability of fatigue data more complicated. Even though NUREG/CR-6909[3] investigates many factors, the influence of welds and other stress raisers are still uncertain.

ASME III provides different levels of analysis. This may lead to different fatigue design lives of a specific component, due to the choice of analysis level. Today, detailed analyses are performed which allows for more detailed resolution of the stresses. The fatigue design process involves many more considerations than just the choice of fatigue curves. Handling of stress raisers, load determination, cyclic plasticity etc, has a large influence on the results. Thus a large part of the real margins in the ASME III procedure are controlled by other factors than those investigated in NUREG/CR-6909 [3].

2.5.2 The applied margins (transferability factors) on the mean curves

The investigation of the applied factors on life in NUREG/CR-6909 [3] is comprehensive. The factor 12 on life in the low cycle regime results from the ANL criterion that the failure probability should be 5% on the component level (see chapter 2.3). However, a failure probability of 5% can seem quite high. The corresponding failure probability in EN 13445-3 [6] is 0.5% (three standard deviations from the mean). No distinct explanation for this choice of probability is given in NUREG/CR-6909. However, the change from factor 20 to 12 on life in itself leads to no significant changes and the difference in the corresponding allowable stresses will be limited. In fact, the differences between the Langer curves and ANL curves for cycles $< 10^4$ are quite small, as shown in Figure 9 and Figure 10.

The investigation of the factors in the high-cycle regime is less penetrating in NUREG/CR-6909 [3]. This is a shortcoming for several reasons. In fact the uncertainties regarding material variability, data scatter, size effects, surface finish etc. are generally greater in the high cycle regime. Not the least important is the well documented tendency of spectrum load to lower the fatigue limit [7]. This means that load levels that do not accumulate fatigue damage in constant amplitude loading may do so as part of a load spectrum. Thus the need for margins in the high-cycle regime is still an open question. It's importance is emphasized since the deviation between the Langer curves and ANL curves are the largest in the high cycle regime. A reasonably valid evaluation is obtained by comparing with the margins in EN 13445-3, where the margins are determined essentially by three standard deviations (3SD) from the mean data. To obtain this, EN 13445-3 establish a constant margin on stress range. This margin is computed for welded material in Figure 12 and is very near a factor of two. Even though the philosophy in EN 13445-3 is different, and the comparison is not strictly valid, this shows that the ASME III margin of a factor of two applied on strains (stresses) in the high cycle regime should be reasonable.

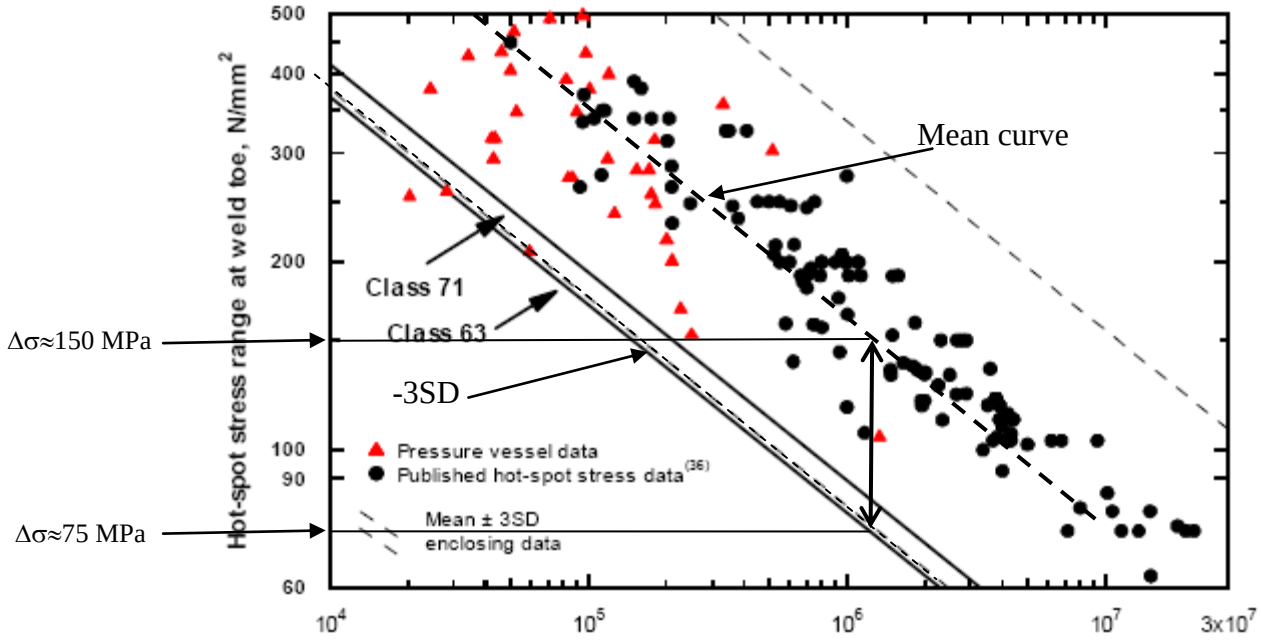

Figure 12. Estimation of margins on stress in EN 13445-3. It is noted that the margin is almost exactly a factor two. Figure from Maddox [8].

2.5.3 The discrepancy for austenitic materials

It has been concluded that the ANL curves, both mean curve and design, have been established by going through a large set of data. Moreover, the potential non-conservatism of the Langer curve had been observer much earlier. Thus there is no reason for questioning the results in NUREG/CR-6909, and the proposed fatigue curves are well supported by the background work.

The conclusion by ANL is that the Langer data are not representative for SS304/SS316 and similar austenitic stainless type steels. It is claimed by ANL that the difference between ANL and the Langer data depends on the higher yield strength for the Langer specimen. It is further claimed that this higher strength is not representative for today's austenitic steels.

Solin et. al. [9] made fatigue tests on X6CrNiNb1810, which correspond to SS347. The tests were performed at VTT in Finland. This type of material is explicitly not included in the ANL data. However, it is customary believed that there is no significant differences between SS347 and SS304/316 in terms of fatigue properties. Solin et. al. claim that their tests show that the Langer data is still valid, and that their material batches are representative for primary loops in certain PWRs. The VTT results are shown in Figure 13 together with the ANL data.

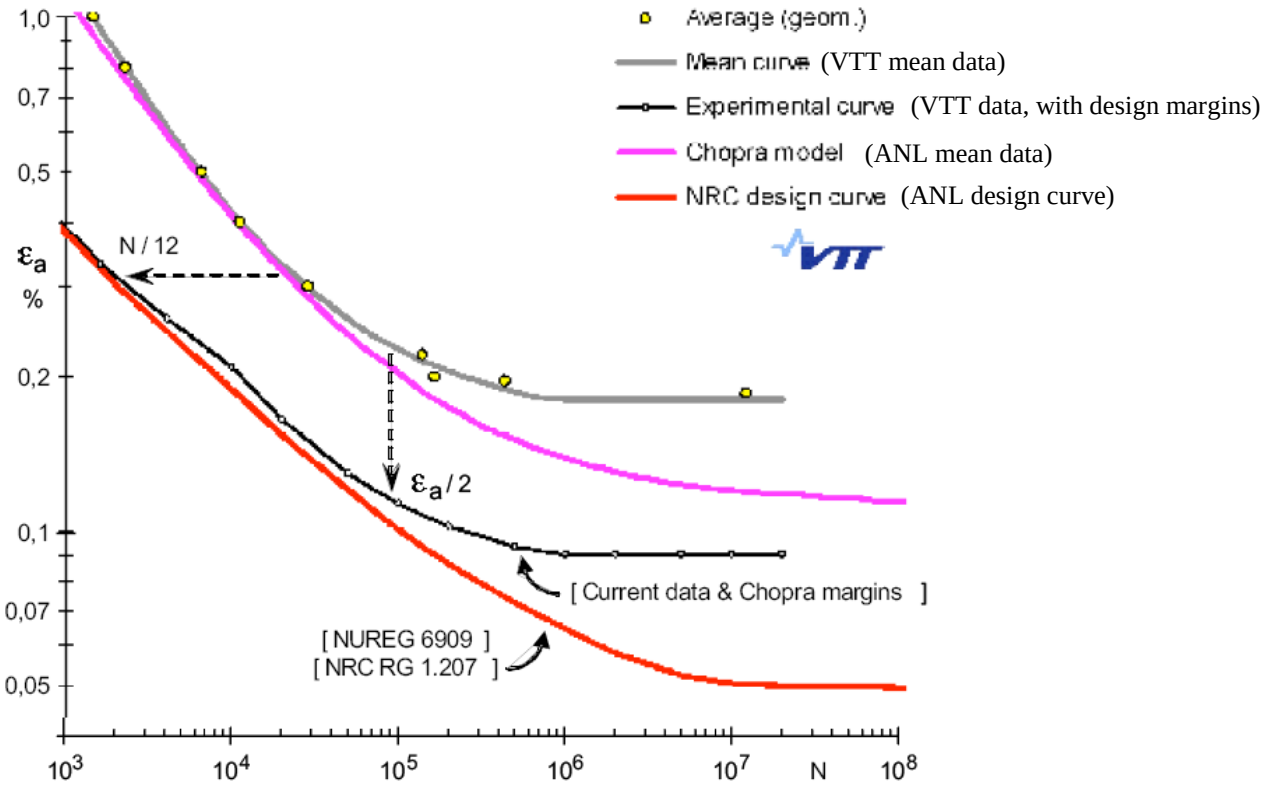

Figure 13. VTT data compared to Langer and ANL. Strain amplitude versus number of cycles to failure. The curve labeled Mean curve and yellow dots refer to the VTT data.

The yield strength of the VTT batch of austenitic material was determined to $R_{p0.2}$ = 240 MPa which is representative of this material. This does not much deviate significantly from the other SS materials 304/316. Hence, high static yield stress is hardly a cause for the difference.

The cyclic hardening data is compared from three sources; ANL [3], VTT [9] and Jiang et. Al. [10], and shown in Figure 14. All three data comes from room temperature cyclic data. Significant for the VTT data is the secondary cyclic hardening, which does not appear for the SS304/316 steels, ANL [3] and Jiang et. Al. [10]. This hardening occurs at all load levels for the VTT data, but is however most prominent for low load levels. For strain amplitudes just below the VTT fatigue limit, $\varepsilon_a = 0.195\%$, the secondary hardening is pronounced from 10^5 load cycles and onwards, see Figure 14. The stress amplitude increases almost 50%. This hardening will significantly decrease the amplitude of cyclic plastic deformation and will significantly increase the fatigue life.

It is suggested by VTT that the HCF properties of X6CrNiNb1810 are improved both by secondary hardening and by a hardening effect from niobium carbides. This may explain the difference between a stabilized austenitic stainless steel and a low carbon grade austenitic steel, such as 304L/316L. To mitigate sensitization and IGSCC the tendency during recent decades was to shift from stabilized medium carbon austenitic stainless steel to low carbon austenitic grades, which may impair the HCF properties.

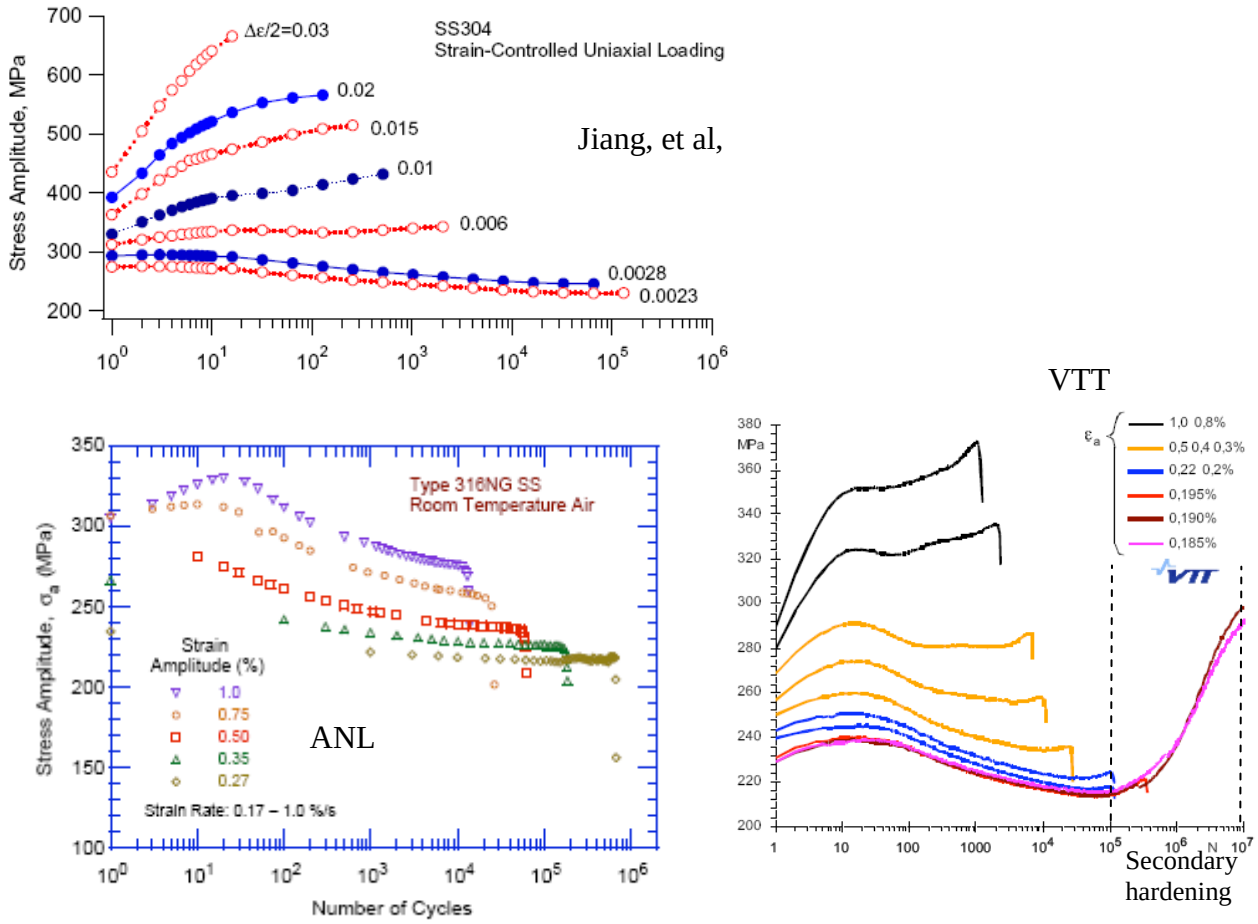

Figure 14. Cyclic strain hardening/softening, ANL [3] and VTT [9] and Jiang [10].

In sum, it is highly likely that the strong secondary cyclic hardening in the VTT experiment is responsible for the higher fatigue strength in the VTT experiments as compared to the ANL data. The presence of cyclic hardening significantly decreases the amount of plastic strains in a prescribed strain load condition, thus decreasing the fatigue damage accumulation. There is no distinct explanation why this effect is prominent for some austenitic steels and not for others. A possible explanation is that the ANL data is supposed to contain mostly low carbon grade austenitic steels, while Langer data is older and, thus, may contain stabilized medium carbon grade austenitic steels, which may be one significant factor to explain the different HCF properties found. Further investigation is recommended. It is argued that component testing, involving realistic parameters, such as welds and variable amplitude loads could be utilized in order investigate the differences between the material types. It should be noted, however, that these differences only occur during constant amplitude loads. It is likely that variable amplitude load conditions will alter the effects of secondary hardening.

2.6 Alternative procedure by EN 13445-3

It is noteworthy that the relatively new European standard EN 13445-3 [6] for non-nuclear pressure vessels has taken an entirely different approach to fatigue. The approach in EN 13345-3 is essentially based on the IIW recommendations [11]. The fatigue curves are based on stress controlled experiments on component-like specimen. The specimens contain different types of configurations or fatigue curves. The approach is essentially the same as used by the general design code Eurocode 3 [[12]13] and several other standards. A main difference is that the design curves in EN 13445-3 are converted to the use of three standard deviations below the mean curve (mean – 3SD) instead of two standard deviations (mean -2SD), as in the other codes, i. e. the IIW recommendations [11] and Eurocode 3 [12].

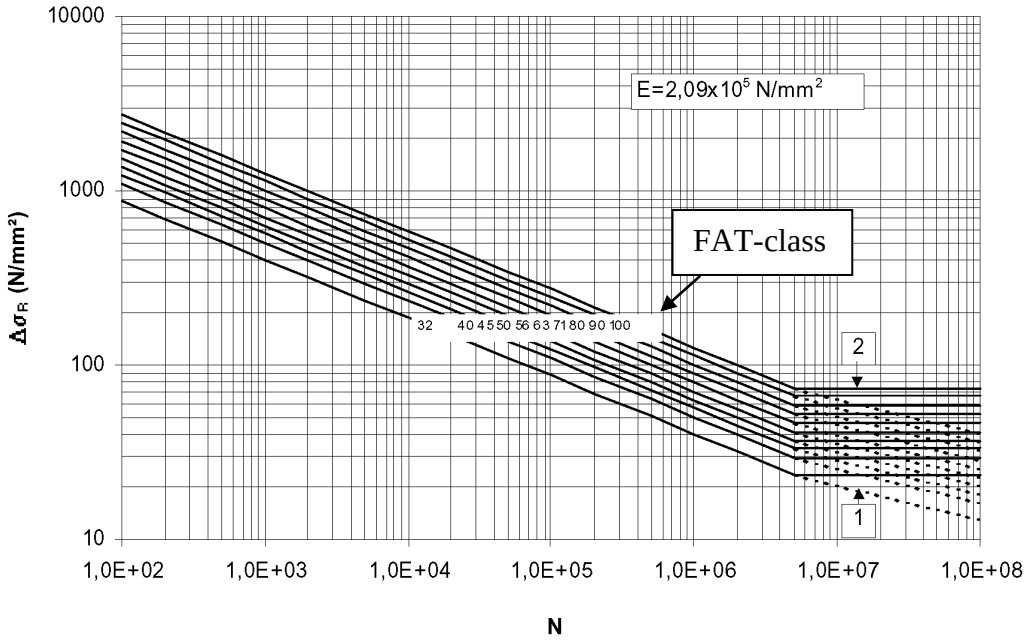

Figure 15. The fatigue design curves in EN 13445. The solid horizontal lines are the constant amplitude fatigue limits. The dotted lines are the curves to use under spectrum loading.

The standard provides a set of fatigue curves, see Figure 15. These curves are based on a statistical treatment of the experiments with different weld configuration, execution and geometry. The fatigue curve is specified by it's FAT-class, which is defined by the stress range at N=2x10^6 cycles. The procedure in EN 13445-3 does not explicitly demands for a fatigue reduction factor for the presence of welds. The influence of a particular weld is instead already included in the specific fatigue curve. The effects are included in the choice of FAT-class. The choice of FAT-class is based on the weld configuration, execution and geometry. EN 13445-3 provides charts and figures from which the FAT-class is determined. The exponent for the fatigue curve is m=3, regardless of FAT-class. Size effects and the influence of temperature are treated by separate correction factors. It is also noted that EN 13445-3 demands an extension of the fatigue curve for spectrum loads. This is done since it has been experimentally demonstrated in several studies that spectrum loads tend to lower the limit for fatigue damage to occur. See for example the study by Marquis [7]. The curve is extended from the constant

amplitude fatigue limit at N=5x10^6 to a cut-off limit at N=10^8, with an exponent of m=5. In terms of stresses, the fatigue limit is lowered by factor of $(5/100)^{1/5} = 0.55$.

The approach in EN 13445-3 has some clear advantages over ASME III. The experiments on realistic specimens make the transferability to real components more accurate. Moreover, the approach has been subjected to several investigations. Probably this has to do with the approach being applied in several industries, where fatigue is a more prominent problem than in the nuclear industry. Hence the applicability of the approach in real applications is well documented. A thorough study was performed by Maddox [8], a study which included pressure vessel and piping components as well as other components. The studies intent was to evaluate the applicability of the procedures in EN 13445-3. Fatigue analysis for un-welded material in EN 13445-3 was initially covered by a special section, were the design curves are based on smooth specimen data, instead of a FAT-class. The fatigue curve is determined by the ultimate strength, which is supposed to correlate to the fatigue limit for smooth specimens. This concept was evaluated by Maddox. The ultimate strength correlation with the fatigue characteristics was much criticized by Maddox [8]. Firstly, Maddox showed that standard steel plates have fatigue characteristics almost equal to welds. See Figure 16 that contains test results for plates with and without welds. There is a potential risk that the smooth specimen concept tends to overestimate the fatigue strength for un-welded material also. Moreover, he showed that there is no experimental evidence from tests on realistic vessel components failing on un-welded material that any distinction should be drawn of different tensile strength. This is in conflict with the ASME design curves for carbon and low-alloy steels in Figure 1, with clearly higher long life fatigue strength for the higher ultimate strength. Maddox proposed a strategy based on the choice of FAT class, regardless of ultimate strength, which is in line with the IIW recommendations. EN 13445-3 now contains this approach as an option. However, the main drawback of the approach in EN 13445-3, is that it is less suited for deformation controlled fatigue as in thermal fatigue. The reason is the stress control load. For accurate thermal fatigue analysis the strain-life relation is needed.

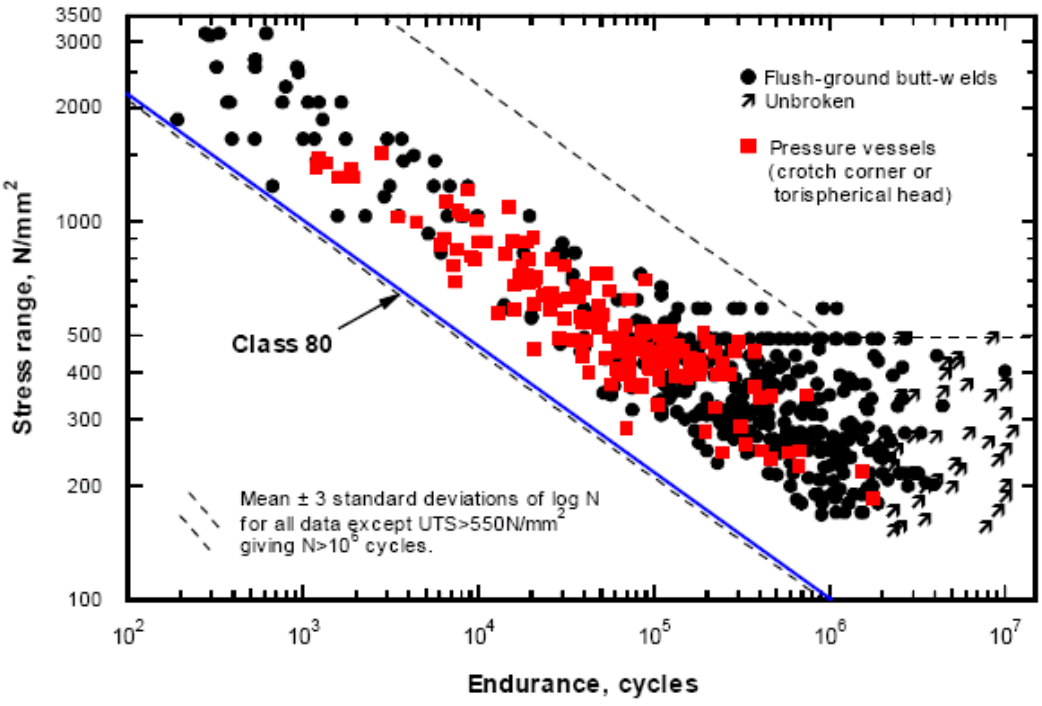

Figure 16. Fatigue results for non-welded material. From Maddox [8]. Note that un-welded material (red squares) have the same fatigue strength as welded material (black dots).

2.7 On margins in fatigue design analyses with ASME

A fatigue design analysis of a real component includes several steps and the analysis can be performed on several levels. For piping, ASME III, section NB3600 for piping presents a methodology that is fairly well defined. Plasticity corrections and fatigue reduction factors are given by tables and formulas, even though their values have been much discussed (see for example Grandemange [14]). ASME III, section NB3200 allows for design by analysis in a much more open way. Elastic analyses or elasto-plastic analysis verification may be performed. Little guidance on details is given. Hence, analysis results may vary, especially since estimation of fatigue reduction of welds and plastic deformation are very difficult. The current ASME fatigue curves include some rather arbitrary choice of curve depending on the presence of welds and means stress as shown in Figure 10. This problem has been solved by the introduction of the ANL curve which only has one curve. However, this curve takes into account full influence of compressive residuals stresses which may be a conservative in many cases.

It is commonly believed that the design loads in the analysis of NPP components are conservative. However, estimation of the conservatism in loads should need a separate investigation. The conservatism in the fatigue design analysis with accurately defines loads should be further investigated. It is notes that the ANL estimation of transferability factors (see Figure 8 and Table 3) assumes exact estimation of stress and strains, fatigue reduction factors etc. Estimation of these factors is a crucial part of fatigue design analysis. The influence of these factors should be further studied in order to considerably improve the understanding of the real conservatism (or lack of it). A suitable set of controlled tests of components should provide benchmark examples. In that respect the ASME procedure is poorly investigated in comparison to the EN 13345-3 for which there exists a generous source of tests for evaluating the procedure. Future studies on aspects on ASME fatigue philosophy should focus less on the small strain controlled specimen, and more on the fatigue of real components. The set-up of real component tests is fairly straight forward.

3 ENVIRONMENTAL EFFECTS IN LWR CONDITIONS

3.1 Background

The effects of environmentally-assisted cracking (EAC) on for example the reactor pressure vessel and pipes are a key concern within the context of both reactor safety and evaluation/extension of plant service life. Based on the external, macroscopic loading conditions, three basic types of EAC can be differentiated; stress corrosion cracking (SCC), strain-induced corrosion cracking (SICC) and corrosion fatigue (CF). In this report we focus on corrosion fatigue, which is caused by cyclic loading (low- or high-cycle). Many failures of reactor components are caused by fatigue, examples are piping, nozzles, valves, control rod driving (CRD) and pumps [15-19]. In feedwater nozzles and piping the mechanism of cracking has been ascribed corrosion fatigue (CF) or strain-induced corrosion cracking (SICC) [15-19].

Subsection NB-3121 of Section III in ASME [1] explicitly notes that the data used to develop the ASME Code fatigue curves did not include tests in the presence of corrosive environments that might accelerate fatigue failure. Article B-2131 states that the owner's design specifications should provide information about any reduction to fatigue design curves that is necessitated by environmental conditions.

3.2 Experimental results

Existing fatigue strain vs. life (ε-N) data illustrates potentially significant effects of LWR coolant environments on the fatigue resistance of carbon and low-alloy steel [20-35] as well as austenitic stainless steels [22, 23, 25, 26, 33, 36-41], see Figure 17. For all three material types, the fatigue life is reduced significantly only when certain parameters meet certain threshold values.

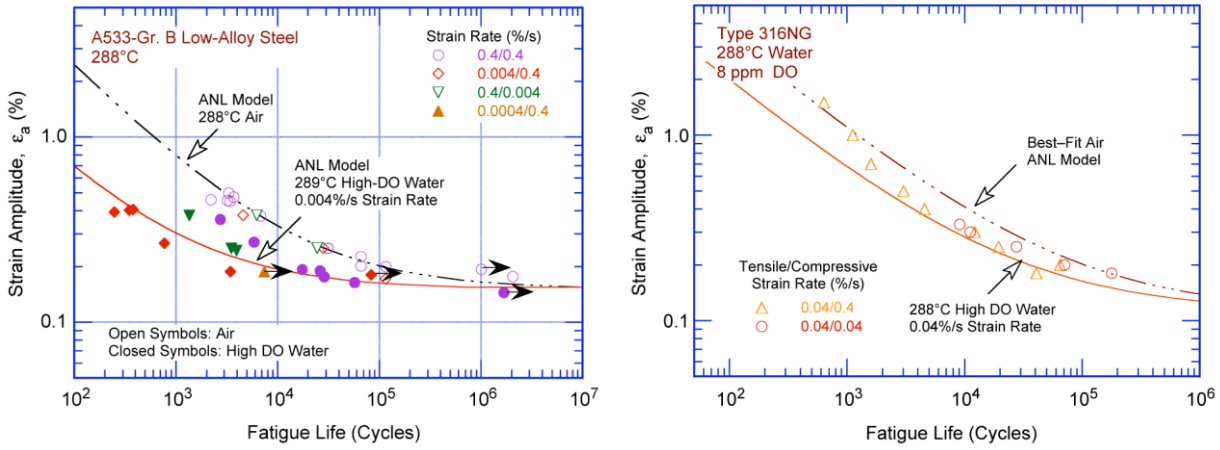

(a) (b)

Figure 17. Strain amplitude vs. fatigue life data for (a) low-alloy steel and (b) austenitic stainless steel [3].

The fatigue data in LWR environments indicate that the key parameters that influence fatigue life in LWR environments for carbon and low-alloy steels are temperature, dissolved oxygen (DO) level in water, strain rate, strain (or stress) amplitude and for carbon and low-alloy steels, sulphur (S) content of the steel. It is shown that a significant decrease in fatigue life of carbon and low-alloy steels is

obtained when four key threshold conditions are satisfied simultaneously; applied strain range, service temperature and dissolved oxygen in the water are above a minimum threshold level, and the loading strain rate is below a threshold value. Although the microstructures and cyclic-hardening behaviour of carbon steels and low-alloy steels are significantly different environmental degradation of fatigue life of these steels is identical.
For both steels, environmental effects on fatigue life are moderate (i.e. a factor of two or lower) if any one of the key threshold conditions is not satisfied [3, 20, 31, 42].

For austenitic stainless steels, the fatigue life is decreased significantly when three threshold conditions are satisfied simultaneously; applied strain range and service temperature are above a minimum threshold level, and the loading strain rate is below a threshold value. The dissolved oxygen level in the water and possibly the composition and heat treatment of the steel are also important parameters for environmental effects on fatigue life [3].

For nickel-base alloys (Ni-Cr-Fe) the existing fatigue data in LWR environments are very limited; the effects of the key loading and environmental parameters on fatigue life of these alloys have been evaluated by Higuchi et al. [43], see Figure 18. The results indicate that environmental effects are strongly dependent on key parameters such as strain rate, temperature and dissolved oxygen level in water [3, 43]. The fatigue life reduction was found to be greater in PWR primary water than in BWR water [43].

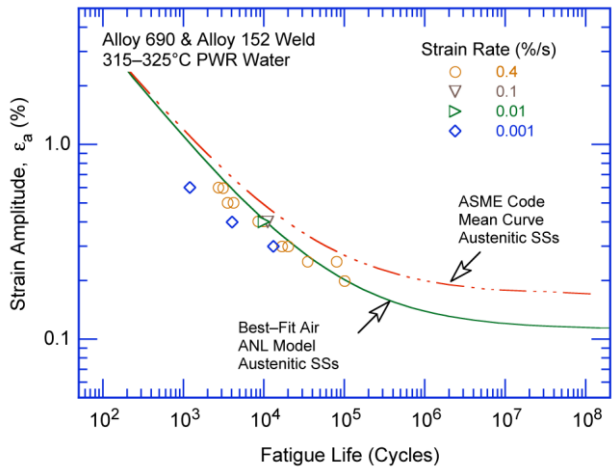

Figure 18. Fatigue behaviour for alloy 690 and 152 Weld in simulated PWR water [3].

Environmental fatigue tests have also been performed for high strength materials (including carbon steel STS480 and low-alloy steel SQV2B). The test results confirmed that the environmental effects are not significant for these high strength materials [44-46].

There are some differences between BWR water and PWR water regarding actual water chemistry and also the temperature conditions [21, 36]. The BWR water is deionised water with very low electrical conductivity while the PWR water contains B (500 ppm) and Li (2 ppm) and indicates higher electrical conductivity [36]. BWR water also has higher dissolved oxygen level and usually lower temperature than PWR. Environmental effects on fatigue life in BWR water is more moderate compared to that in PWR water for austenitic stainless steel [36].

A great number of tests have been conducted mainly in Japan to identify and quantify the effects of environmental parameters [21-25, 27-34, 36, 38, 39, 43, 44, 47] but also in USA [20, 26, 35, 37, 38, 48] and some in Switzerland [40, 41, 49, 50]. All experiments are consistent with each other except for small differences, see below.

3.2.1 Strain range

A minimum threshold strain range is required for environmentally assisted decrease in fatigue life for carbon and low-alloy steels as well as austenitic stainless steels [20, 35, 48]. The threshold strain range appears to be almost independent of material type (weld metal or base metal) and temperature in the range of 250-325˚C [48]. Experiments on carbon and low-alloy steel indicate that the fatigue life reduction is independent of strain amplitude once the amplitude exceeds a threshold value [20] which most likely corresponds to rapture of the passive surface oxid film [20, 35, 38]. This need not imply that the observed threshold strain is the actual film rupture strain. Film rupture occurs at the crack tip and is controlled by the crack tip strain. The existing data for Ni-Cr-Fe are inadequate to define the threshold strain amplitude below which environmental effects on fatigue life do not occur, although experiments on carbon and low–alloy steels by Chopra and Shack showed threshold strain range at approximately 0.36%, see Figure 19.

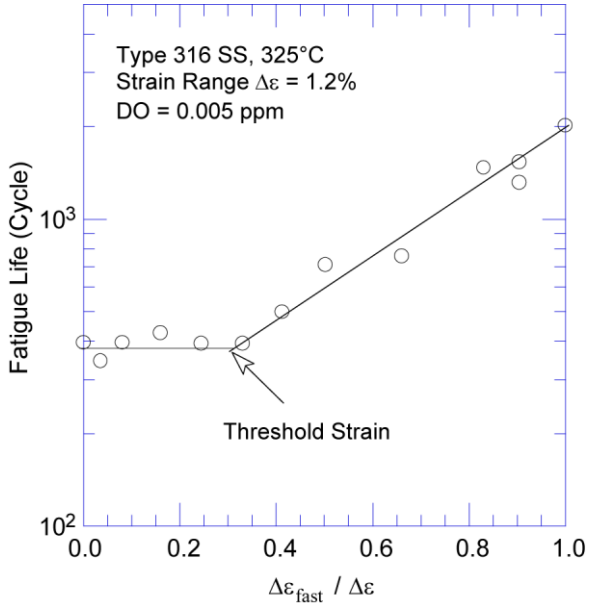

Figure 19. Fatigue life plotted as a function of fraction of strain at high strain rate [48].

3.2.2 Strain rate

The effect of strain rate on fatigue life of carbon, low-alloy and austenitic steels in LWR environments is significant when the strain rate is positive and other key thresholds conditions, i.e. strain amplitude, temperature and dissolved oxygen content, are satisfied, see Figure 20 and Figure 21. When all threshold conditions are satisfied, the logarithm of fatigue life decreases linearly with decreasing logarithmic strain rate at least below 1%/s for carbon and low-alloy steels and below 0.4%/s for austenitic steels [3, 21, 28, 35, 43, 44, 47]. Because of the limited data for Ni-Cr-Fe the threshold strain rate below which environmental effects are significant cannot be determined from the present data, although it can be seen that the fatigue life of these alloys decreases linearly with decreasing strain rate [3, 43, 44, 47]. It was also found that the effects of water on the fatigue of Ni-base alloys were much smaller than for stainless steels [43].

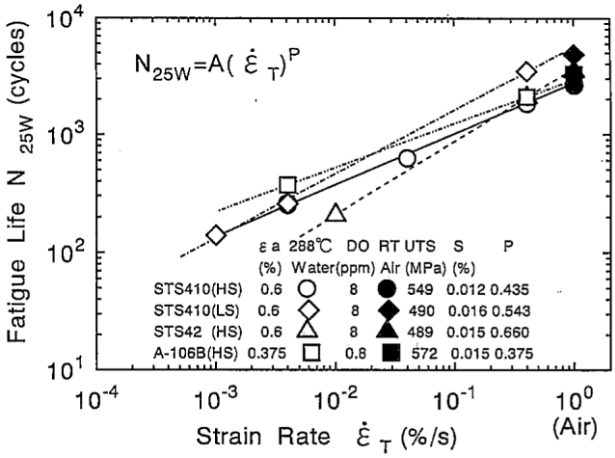

Figure 20. Relation between strain rate and fatigue life for carbon steel [28].

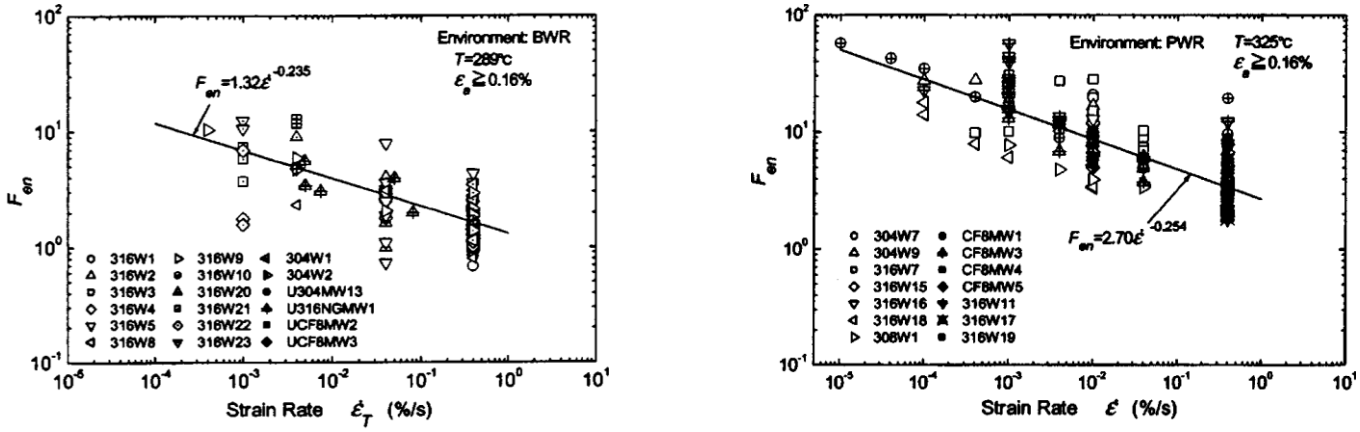

(a) (b)

Figure 21. Relation between F_{en} (N_{air}/N_{water}) and strain rate in (a) BWR water and (b) PWR water [36].

The existing fatigue data indicate that a slow strain rate applied during the tensile-loading cycle is primary responsible for environmentally assisted reduction in fatigue life of these steels [3, 20, 35, 38]. Higuchi et al [28] has concluded that the strain rate in the strain decreasing part of the cycle does not affect the environmental fatigue life unless it becomes smaller than that of the increasing straining part of the cycle.

Higuchi et al [28, 33] have performed a series of strain controlled fatigue tests with the strain rate changed stepwise by three different waveforms (fast/slow-convex, slow/fast-concave, sawtooth) or continuously. It is shown that constant strain rate gives the shortest fatigue life if the rise time is the same and that taking the strain rate as average over the minimum to peak of the strain change is a conservative method. They stated that damage evaluation conducted based on the partial slow strain rate in the transient period will allow the cumulative damage to become excessively high. Higuchi et al. [33] have also performed fatigue tests with sine wave straining and the fatigue life of sine wave tests were always much higher than those of stepwise wave tests at the same rise time and strain amplitude.

Strain rate due to a thermal transient under actual plant operation is usually much less than 1 %/s, while strain rate due to an earthquake would considerably exceed 1 %/s [36]. Environmental effects are not considered for seismic loads since seismic load cycles are characterised by high strain rates of short duration [36, 44]. High-cycle fatigue due to high-frequency vibrations also has strain rates that are too high for significant environmental effects [40, 41].

3.2.3 Temperature

Experimental results indicate a threshold temperature of 150-160˚C, above which the fatigue life decreases, see Figure 22. In the temperature range 150-320˚C for carbon and low-alloy steels and 150 (/200)-325˚C for austenitic steels, the logarithm of fatigue life decreases linearly with increasing temperature [3, 20, 29, 30, 38, 43, 44], see Figure 22. A large part of the experiments have been conducted at temperatures between 260 and 325˚C [48]. However, according to JSME [44], a similar behaviour is also seen for temperatures below 50˚C for carbon and low-alloy steels, although the environmental effect is significantly less for those temperatures. For Ni-Cr-Fe alloys the existing data are inadequate to determine accurately the effect of temperature on fatigue life although increasing temperature reduces the fatigue life [43, 44, 47].

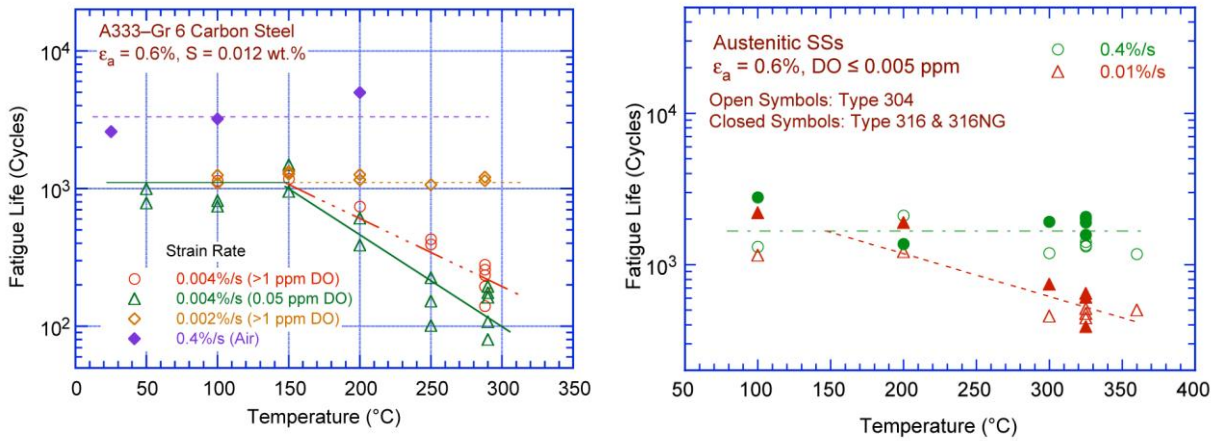

(a) (b)

Figure 22. Change of fatigue life with temperature for (a) carbon steel and (b) austenitic stainless steel [3].

Kanasaki et al. [30] have performed an experimental study to examine the effects of thermal strain cycling synchronously combined with mechanical cycling in the manner of in-phase and out-of-phase, see Figure 23. The wave shape of strain cycling was triangular with three different temperature ranges, 50˚C to 290˚C, 50˚C to 200˚C and 200˚C to 290˚C. Fatigue life tended to decrease for increasing temperature above 200˚C. The results showed that the fatigue lives at temperature range of 50˚C to 290˚C and 200˚C to 290˚C were in the range between fatigue life at the lowest temperature and that at

the highest temperature in each temperature cycling- It was also found that fatigue life of the in-phase test was equal to that of the out-of-phase test.

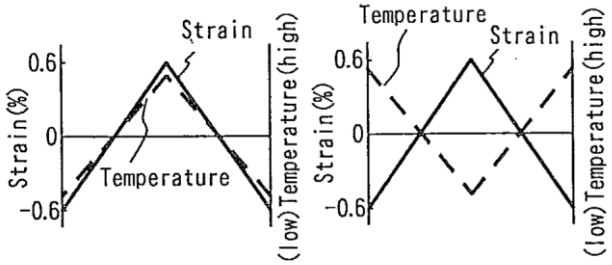

Figure 23. Pattern of temperature and strain change [30].

3.2.4 Dissolved Oxygen

Experiments have shown a minimum dissolved oxygen level in water of 0.03-0.05 ppm above which environment decreases the fatigue life of carbon and low-alloy steels. The data shows an approximate linear dependence between the logarithm of fatigue life and the logarithm of dissolved oxygen level. The effect of dissolved oxygen content on fatigue life saturates at 0.5-1 ppm, i.e. increases in dissolved oxygen levels above 0.5-1 ppm do not cause further decreases in life [3, 20, 29, 43, 44], see Figure 24. Effect of dissolve oxygen concentration on fatigue crack growth rates in BWR conditions has also been investigated. The fatigue crack growth rates showed almost independence of dissolved oxygen concentration below 1 ppm, while above 1 ppm striking dissolved oxygen dependence was observed and the crack growth rate increased with increasing dissolved oxygen concentration [34].

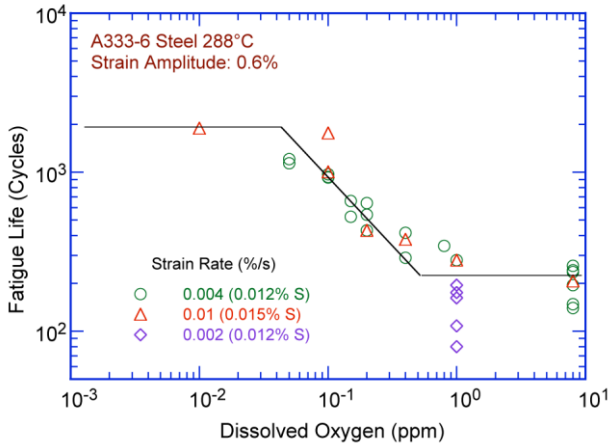

Figure 24. Dependence on dissolved oxygen of fatigue life for carbon steel [3].

In contrast to the behaviour of carbon and low-alloy steels, the fatigue lives of austenitic stainless steels decrease significantly in low-DO water (i.e. < 0.05 ppm dissolved oxygen). In high-DO water, the fatigue lives of austenitic stainless steels are either comparable to or, in some cases, higher than those in low-DO water [37-39, 48, 47]. There is no clear dependency on the dissolved oxygen concentration [38, 44, 47]. Similar results are shown for Ni-Cr-Fe alloys as for austenitic stainless steels [3, 43, 44, 47]. The effects of loading and environmental parameters on the fatigue life of cast stainless steels differ somewhat from those on wrought stainless steels. Existing data indicate that the

fatigue lives of cast stainless steels are comparable to those observed for wrought in low-DO water [48].

In all environments, cracks in austenitic stainless steels primarily form within persistent slip bands. Once a microcrack is formed, it continues to grow along its slip plane as a Mode II (shear) crack in Stage I growth. The orientation of the crack is usually at an angle 45˚ to the stress axis. The Stage I crack may extend across several grains before the increasing stress intensity of the crack promotes slip on systems other than the primary slip. The crack begins to propagate as a Mode I (tensile) crack, normal to the stress axis in Stage II growth. From the experiments performed by Chopra and Gavenda [31, 37] this behaviour was observed in all of the specimens tested in air and in most occasions for specimens tested in high-DO water, see Figure 25. However, in simulated PWR environment (< 0.01 ppm dissolved oxygen) the surface cracks appeared to grow entirely as Mode I (tensile) cracks normal to the stress axis, see Figure 25. In another study both tests in PWR and BWR environments showed a crack initiation and crack growth normal to the stress axis [39].

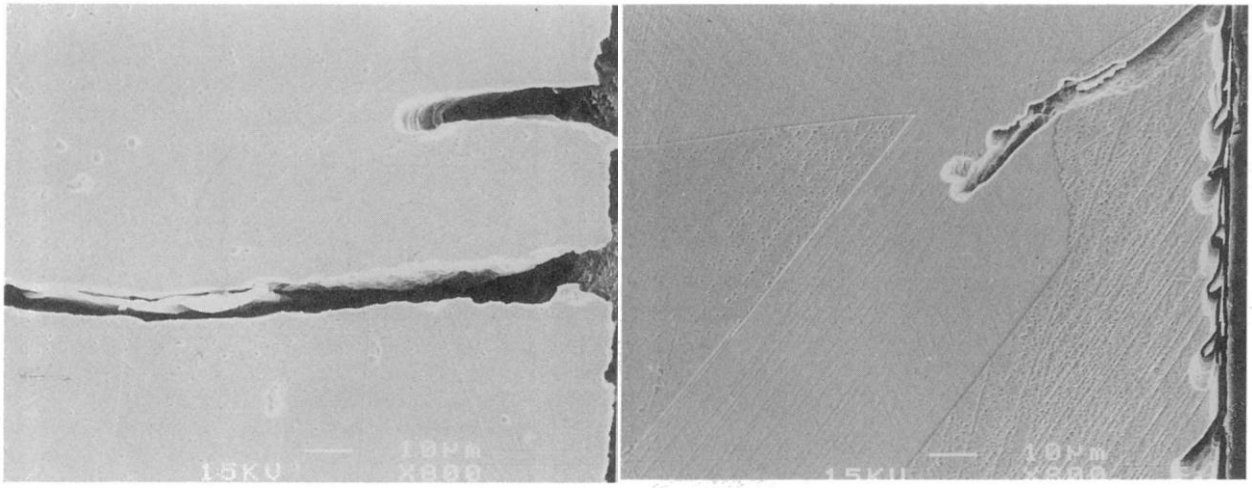

(a) (b)

Figure 25. Photomicrographs of surface cracks of Type 316 NG stainless steel tested in 288 in (a) low- (< 0.01 ppm) and (b) high-DO water (0.7 ppm).

3.2.5 Sulphur

When all the threshold conditions are satisfied, environmental effects on the fatigue life for carbon and low-alloy steels increases with increased sulphur content [3, 43, 44], see Figure 26. However, the available data sets are almost too sparse to establish a functional form for dependence of fatigue life on sulphur content and to define either a threshold for sulphur content below which environmental effects are unimportant or an upper limit above which the effect of sulphur on fatigue life may saturate [3]. The limited data suggest that environmental effects on fatigue life saturate at sulphur contents above 0.012-0.015 wt. % [20]. The logarithm of the environmental fatigue life correction factor appears to increase linearly with sulphur content [44].

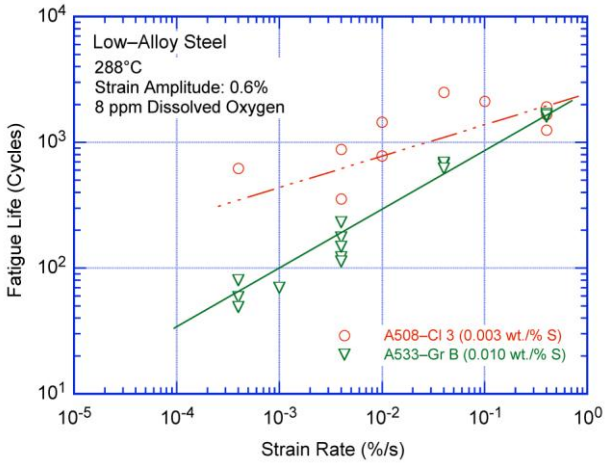

Figure 26. Effect of strain rate on fatigue life of low-alloy steels with different sulphur content [3].

Hänninen et al. [51] have done an experimental study on two different materials to investigate the micro mechanisms of environmental cyclic crack growth, hydrogen-induced cracking. In the study the two different material selected (A533B C1.1 pressure vessel steel and Cr-Mo-V pressure vessel steel) have almost the same sulphur content but they have, among other things, marked differences in MnS (manganese sulphide) inclusion morphology and distribution. In the study it seemed that a change in the form, size and distribution of MnS inclusions would have much larger effect on the crack growth rate than sulphur content. Thus, inclusion shape control to minimize the anisotropy of the steel seems to be more important than the cleanliness of the steel.

3.2.6 Flow rate

Nearly all of the fatigue data for LWR environments have been obtained at very low water flow rates [3]. Data indicate that for high sulphur carbon steel (S = 0.016 wt%) in LWR environments with dissolved oxygen > 0.01 ppm and slow strain rates the environmental effects on the fatigue life are at least a factor of 2 lower at high flow rates (7 m/s) than at 0.3 m/s or lower [22-25, 44], see Figure 27. In low sulphur carbon steel (S = 0.008 wt%) and in low-alloy steel (S = 0.008 wt%) the fatigue lives in a water flow rate of 7 m/s were almost the same as those in stagnant water even though there was a tendency for an increase in fatigue life [22, 23, 25]. Flow rate seems to have no effect on fatigue life in PWR [44].

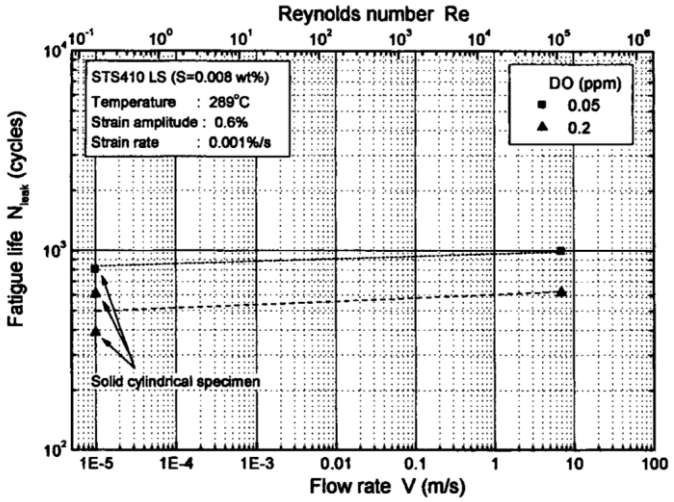

Figure 27.Effect of water flow rate on fatigue life of carbon steel [23].

The mechanism responsible for the mitigation of fatigue life reduction is suggested to be the flushing effect of the water which exchanges the corrosive water in the crack and thereby eliminates the locally corrosive environment. [22-25]. This increase in fatigue life is attributed to increases in the crack initiation life and small-crack propagation life, although differences in crack propagation rate were observed for the whole crack propagation process [24, 25, 28]. The local corrosive environment of low sulphur carbon steel is considered to be less severe than that of high sulphur carbon steel. Therefore water flushing may play a less important role for low sulphur carbon steel [22, 23]. The results suggests that the environmental fatigue life under various flow rate conditions should be determined by the combination between the mitigating effect caused by flushing of the severe local environment and the enhancing effect caused by increase in corrosion potential.

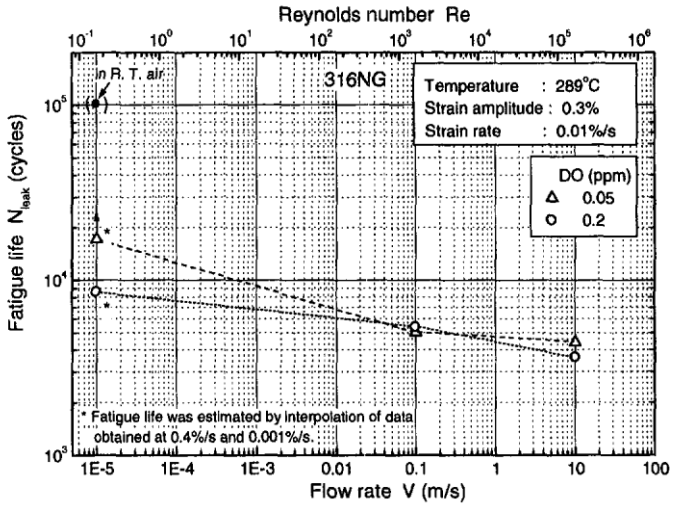

Figure 28. Effect of water flow rate on fatigue life of austenitic stainless steel [22].

Contrary to carbon steel, in austenitic stainless steels the fatigue can even become shorter for high flow rate, see Figure 28, but with large data scatter it is impossible to quantify the dependency on the flow rate [22, 23, 25, 44]. Water flushing may have a moderate effect [22, 23]. For 316NG stainless steel the fatigue life difference was insignificant between the different water flow rates irrespective of

dissolved oxygen level, while for 304 and 304L stainless steels noticeable fatigue life decrease with an increase in water flow rate is noted irrespective of dissolved oxygen concentration. The difference of the behaviour between 316NG and 304 may be from difference of corrosion behaviour. The oxide film was analysed and measured by Raman spectroscopy. It was found that in 304 the ratio inside film thickness/outside film thickness decreased with an increase in flow rate, while the ratio was constant for 316NG. The inside oxide film is the layer which exists adjacent to the metal surface and is considered the main barrier of the corrosive environment [25].

Because of the uncertainties in the flow conditions at or near the locations of crack initiation and the moderate effect of flow rate, flow rate effects on the fatigue life is presently not included in fatigue evaluations [3, 44, 47].

3.2.7 Strain holding

In the BWR environment, the fatigue life of carbon and low-alloy steels is reduced due to strain holding at the peak (local maximum value), see Figure 29. The reduction is significant at higher strain rates while it becomes negligible at the strain rate 0.004 %/s or less. The fatigue life reduction due to strain holding in low-alloy steels is smaller than that in carbon steel. Contrary to the case of carbon steel, the fatigue life reduction due to strain holding at the peak is significant at lower strain rates and disappears at 0.004 %/s or higher strain rates. The extent of fatigue life depends on hold time but tends to saturate as the hold time becomes longer [33, 44]. In BWR the fatigue life reduction of stainless steel is remarkable at a strain rate slower than 0.004%/s [33]. In the PWR environment, the fatigue life of stainless steel is independent from the effect of strain holding [33, 44]. Chopra and Shack [20] have also shown results that indicate that a hold period at peak tensile strain decreases fatigue life in high-DO water. Additional and even contradictory results for hold time effects are given in references [52] and [53]. Continuing examination of hold time effects is recommended.

In actual thermal transients, strain is not usually held at the peak of straining cycle but at a point somewhat reduced from the peak after the stabilization of temperature. In considering this Higuchi et al. [33] performed additional fatigue tests in which the strain was held at a point somewhat reduced from the peak. It was found that under such conditions in BWR environments, the fatigue life reduction caused by strain holding disappeared, see Figure 29. The same tests in simulated PWR water did not either show any fatigue life reduction caused by strain holding. Based on the results of the peak strain hold and sub-peak strain hold fatigue tests, the effect of strain holding on fatigue does not have to be considered for normal thermal transients, but should be considered for transients in which the elastic follow-up stress such as internal pressure is held at peak for long time.

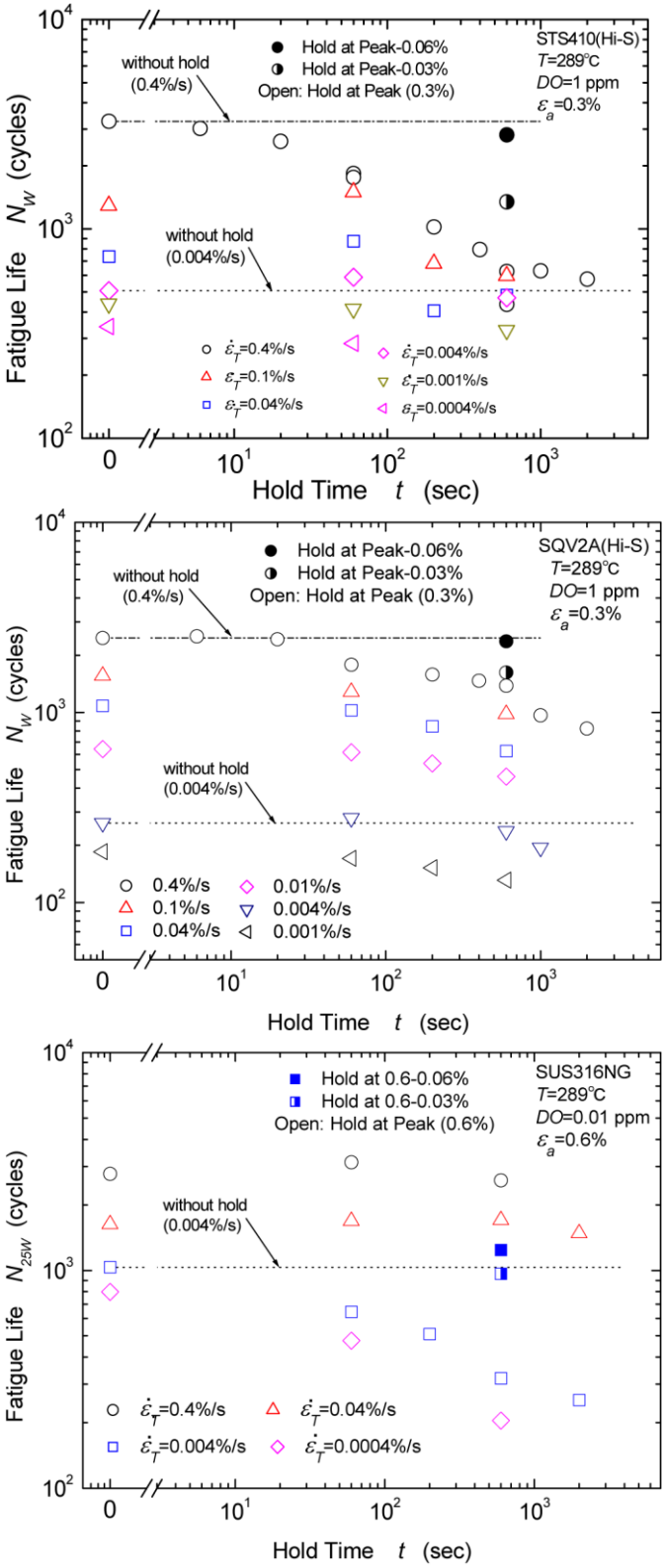

Figure 29. Relation of fatigue life to hold time for (a) carbon steel, (b) low alloy steel and (c) stainless steel in BWR water [33].

3.2.8 Surface roughness

Chopra and Shack [26, 39] have examined the effects of surface roughness on the fatigue life of carbon and low-alloy steels and austenitic stainless steels in air and LWR environments (high- and

low-DO water). For austenitic stainless steels the fatigue life of roughened specimens is a factor of approximately three lower than it is for the smooth specimens in both air and low-DO water. In high-DO water the fatigue life is the same for rough and smooth specimens. The fatigue life of roughened specimens of carbon and low-alloy steels in air and low-DO water is lower than that of smooth specimens, although in low-DO the effect is modest. In high-DO water the fatigue life of roughened and smooth specimens is the same. This could mean that the surface finish transferability factor that is applied on fatigue data in air may be unnecessary in high-DO water (BWR environment). It can be concluded that the effect of surface roughness is small for carbon and low-alloy steels in LWR environments.

3.2.9 Heat treatment

Chopra et al. [39] have performed fatigue tests on austenitic stainless steels (type 304) in LWR coolant environments to examine the effect of heat treatment. The experiments indicate that heat treatment has little or no effect on the fatigue life in air and low-DO PWR environments. In a high-DO BWR environment fatigue life is lower for sensitized stainless steels and the decrease in life appears to increase as degree of sensitization is increased, see Figure 30.

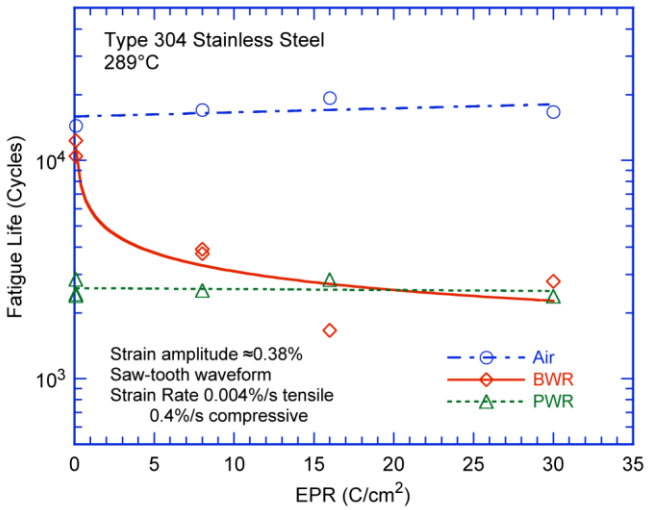

Figure 30. The effect of material heat treatment on fatigue life of Type 304 stainless steel in air, BWR and PWR environments [39]. The EPR (electrochemical potentiodynamic reactivation) value is a measurement of the heat treatment and is dependent on the heat treatment temperature and time.

A detailed metallographic evaluation of the fatigue test specimens was performed. In air, irrespective of the degree of sensitization, the fracture mode for crack initiation and crack propagation is transgranular, most likely along crystallographic planes, leaving behind relatively smooth facets. In the BWR environment the initial crack appeared intergranular, normal to the tensile axis for all heat treatment conditions, implying a weakening of the grain boundaries. Within 200 μm, the initial intergranular mode transformed into a transgranular mode. It appears however that the size of the intergranular portion of the crack surface increased with the degree of sensitization. For all samples tested in PWR environments, the cracks initiated and propagated in a transgranular mode irrespective of the degree of sensitization. The initiation was normal to the tensile axis.

3.2.10 Crack initiation and crack growth

Studies on the formation and growth characteristics of short cracks in smooth fatigue specimens in LWR environments indicate that the decrease in fatigue life is caused primarily by the effects of the environment on the growth of microstructurally small cracks (MSCs), i.e. cracks < 200 μm deep and to a lesser extent on the growth of mechanically small cracks, i.e. the propagation stage [20, 31, 35, 48]. This can be connected to the fact that the growth of MSCs is very sensitive to microstructure while fatigue cracks greater than a critical length, the mechanically small cracks, show little or no influence of microstructure [31]. Chopra and Shack [20, 35, 48] has performed tests in air and high-DO water on carbon and low-alloy steel and examined the crack frequency. For similar loading conditions, the number of cracks in the specimens is identical, see Figure 31, although the fatigue life is lower by a factor of approximately eight in water. If the reduction in life is caused by increased crack formation, the specimens tested in high-DO water should show more cracks. Gavenda et al. [31] have found similar results, i.e. that the environmental appears to have little or no effect on the formation of microcracks.

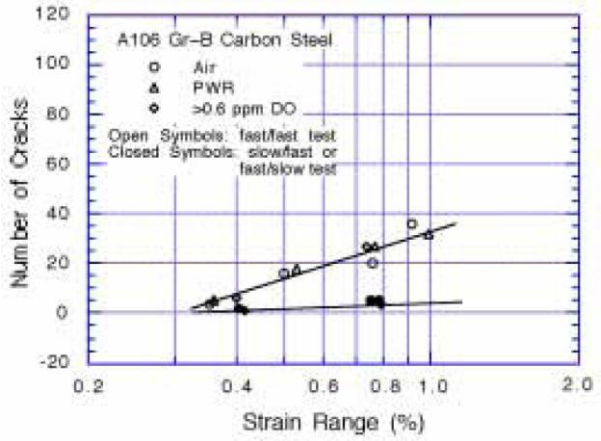

Figure 31. Number of cracks on fatigue specimens tested in different environments [20].

Seifert and Ritter [40, 41, 49] have examined the corrosion fatigue initiation and short crack growth of different low-carbon and stabilized austenitic steels under simulated BWR water chemistry and PWR conditions by cyclic fatigue tests with sharply notched fracture mechanics specimens in the temperature range from 70 to 320˚C. A relevant environmental reduction of fatigue initiation (average crack advance from notch-root of about 10 μm) life occurred for the combination of temperatures ≥ 100˚C, notch strain rates ≤ 0.1 %/s and notch strain amplitudes ≥ 0.3 %, see Figure 32. If these threshold conditions were satisfied simultaneously the environmental enhancement increased with decreasing strain rate and increasing temperature. For example, the corrosion fatigue crack growth rates were increased by a factor of about 5 to 10 with increasing temperature from 150˚C to 320˚C, under comparable loading conditions in air the fatigue crack growth rates increased only by a factor of 1.4. Material properties (such as cyclic plastic behaviour, yield strength, mean grain size, delta-ferrite content, twin boundary fraction, austenite stability, carbides, homogeneity and anisotropy), product form (piping, rod, plate) and water chemistry parameters usually only had a little effect on crack initiation and short crack growth. The effect of environment on the genuine initiation process was relevantly stronger than on the subsequent stationary short crack growth, by a factor of 5 to 10.

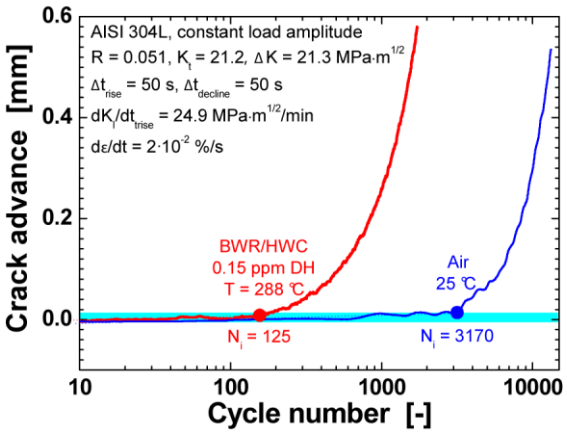

Figure 32. Comparison of fatigue initiation and short crack growth behaviour in air and BWR environment at 288˚C [40].

Seifert and Ritter [40, 41] also found that the effect of temperature on corrosion fatigue crack initiation and short crack growth in austenitic stainless steel at small strain/stress amplitudes was opposite to the usual behaviour, i.e. the environmental reduction decreased with increasing temperature. This is probably related to the distinct secondary hardening at small strain amplitudes and high temperatures due to dynamic strain aging.

In another study [50] the fatigue crack growth behaviour of low-alloy steels was examined. It was found that the crack growth rate increased with increasing temperature from 150˚C to 200˚C. Depending on the loading conditions, the dissolved oxygen level either had very pronounced or only a moderate effect on corrosion fatigue crack growth. Below a loading frequency of 10 Hz, environmental acceleration of fatigue crack growth was observed. Above a dissolved oxygen concentration of 0.4 ppm, neither the dissolved oxygen concentration nor the sulphate content had an effect on the corrosion fatigue crack growth rate.

3.2.11 Mechanism

The environmental effects on the fatigue life of carbon and low-alloy steel are consistent with the slip oxidation/dissolution for crack propagation [54], see Figure 33. A critical concentration of sulphide (S^{2-}) or hydrosulphide (HS^{-}) ions, which are produced by the dissolution of sulphide inclusions in the steel, is required at the crack tip for environmental effects to occur. The crack tip is supplied with sulphide and hydrosulphide ions as the advancing crack intersects the sulphide inclusions and the inclusions dissolve in the high-temperature water environment. Dissolution of MnS inclusions changes the water chemistry near the crack tip, making it more aggressive. The requirements for this mechanism are that a protective oxide film is thermodynamically stable to ensure that the crack will propagate with a high aspect ratio without degrading into a blunt pit, and that a strain increment occurs to rupture that oxide film and thereby expose the underlying matrix to the environment. Once the passive oxide film is ruptured, crack extension is controlled by dissolution of freshly exposed surface and by the oxidation characteristics. The effect of the environment increases with decreasing strain rate. The mechanism assumes that environmental effects do not occur during the compressive load cycle, because during that period water does not have access to the crack tip although limited data indicate that a slow strain rate during the compressive load cycle also slightly decreases fatigue life [20, 38].

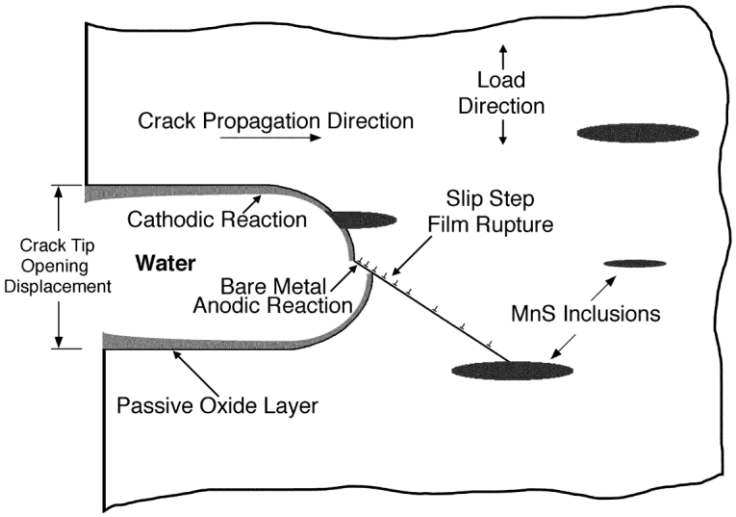

Figure 33. Schematic illustration of film rapture/slip dissolution process [38].

For some austenitic stainless steels the fatigue life is longer in high-DO water than in low-DO PWR environments. Lower fatigue lives in low-DO water than in high-DO water are difficult to reconcile in terms of slip oxidation/dissolution mechanism, which assumes that crack growth rates increase with increasing dissolved oxygen concentration in the water [3, 37, 38]. Similar results are shown for Ni-Cr-Fe alloys. Metallographic examination of the test specimens indicated that environmentally assisted reduction in fatigue lives of austenitic stainless steels most likely is not caused by slip oxidation/dissolution but some other process, such as hydrogen-induced cracking. The presence of well defined striations suggests that the enhanced crack growth rates in austenitic stainless steels are most likely due to hydrogen-induced cracking. Fatigue striations should not be observed if enhancement of crack growth is caused by the slip oxidation/dissolution process [37, 38, 48]. Hydrogen-induced cracking occurs when hydrogen produced by the oxidation reaction at or near the crack tip is partly absorbed into the metal. The absorbed hydrogen diffuses ahead of the crack tip and interacts with MnS inclusions. The MnS inclusions dissolve and the crack tip environment becomes aggressive and conductive to hydrogen absorption. This leads to the formation of cleavage cracks at the inclusion matrix interface. Linkage of the cleavage cracks results in discontinuous crack extension in addition to extension caused by mechanical fatigue [20, 37, 38, 51]. At high hydrogen input rates brittle crack growth also occurs showing a brittle fracture surface morphology (“brittle” striations and cleavage-like fracture) [51]. Other hydrogen-induced fracture processes may also enhance growth rates, for example hydrogen can cause localized crack tip plasticity by reducing the stress required for dislocation motion [48].

Carbon and low-alloy steel specimens tested in water show surface micropitting and cavities that is formed either by corrosion of the material in oxygenated water or by selective dissolution of MnS or other inclusions. These micropits can act as sites for the formation of fatigue cracks. Chopra and Shack [20, 48] has performed tests in specimens preexposed at 288˚C for 30-100 h in water with 0.6-0.8 ppm dissolved oxygen (high-DO water) and then tested in air. It is shown that fatigue lives of the preoxidized specimens are identical to those of unoxidized specimens. If the presence of micropits was responsible for reduction in fatigue lives in LWR environments, then specimens preexposed to high-DO water and then tested in air should also show a decrease in fatigue life.

3.3 Models

Two approaches have been proposed [3, 21, 26, 27, 36, 43, 47, 48, 55, 56] for incorporating the environmental effects into ASME section III fatigue evaluations:

I. Develop new fatigue design curves for LWR applications.
II. Use an environmental fatigue correction factor.

The first approach follows the same procedures used to develop the current fatigue design curves of the ASME code. In this approach, environmentally adjusted fatigue design curves are developed from fits to experimental data. The drawback with this method is that since the metals depend on several loading and environmental parameters, a quite large number of design curves must be developed to cover all possible conditions encountered during plant operation.

The second approach, first proposed by Higuchi et al. [21, 27], uses an environmental fatigue correction factor, F_{en}, which is defined as the ratio of fatigue life in air at room temperature $N_{air,RT}$ to that in water under reactor operating conditions N_{water},

$$F_{en,nom} = N_{air,RT} / N_{water} \ . \tag{3}$$

To incorporate environmental effects into fatigue evaluations the fatigue usage factor for a specific stress cycle or load pair, based on the ASME Code design curves, is multiplied by the environmental fatigue correction factor.

Two specific models are further examined. The models by JSME [47] and Argonne National Laboratory (ANL) [3] are using the second approach.

3.3.1 Model proposed by JSME

The Japan Power Engineering and Inspection Corporation (JAPEIC) suggested models for the environmental fatigue life correction factor in 1999 for carbon and low-alloy steel [56], 2003 for austenitic stainless steel [36] and in 2006 for nickel base alloys [43]. The research project was later being taken over by the Japan Nuclear Energy Safety Organization (JNES) and the models were further developed [55] and a final proposal was presented in 2007 [47]. The JSME (The Japan Society of Mechanical Engineers) models is based on a quite large number of experiments from Japan [25, 33, 43, 45, 46, 57-59] and the Japanese database for fatigue experiments on structural materials at nuclear power plants, the JNUFAD database [60].

3.3.1.1 Carbon and low-alloy steels

The environmental fatigue life correction factor in the final proposal [47] is presented by

$$\ln(F_{en}) = 0.00822(0.772 - \dot{\varepsilon}^*)S^*T^*O^* \tag{4}$$

for carbon and low-alloy steels, where the parameters dependent on the strain rate, $\dot{\varepsilon}$, the dissolved oxygen content in the water, *DO*, the sulphur content in the steel, *S* and the temperature, *T* are defined as

$$\dot{\varepsilon}^* = \ln(2.16) \qquad \text{if } \dot{\varepsilon} > 1\%/\text{s}$$

$$\dot{\varepsilon}^* = \ln(\dot{\varepsilon}) \qquad \text{if } DO \le 0.7 \text{ ppm and } 0.0004 \le \dot{\varepsilon} \le 2.16 \ \%/\text{s}$$

$$\text{or } DO > 0.7 \text{ ppm and } 0.0001 \le \dot{\varepsilon} \le 2.16 \ \%/\text{s}$$

$$\dot{\varepsilon}^* = \ln(0.0004) \quad \text{if } DO \le 0.7 \text{ ppm and } \dot{\varepsilon} < 0.0004 \text{ %/s}$$
$$\dot{\varepsilon}^* = \ln(0.0001) \quad \text{if } DO > 0.7 \text{ ppm and } \dot{\varepsilon} < 0.0001 \text{ %/s}$$

$$S^* = \ln(12.32) + 97.92S$$

$$T^* = 0.0358T \quad \text{if } T < 50^\circ\text{C}$$
$$T^* = \ln(6) \quad \text{if } 50^\circ\text{C} < T < 160^\circ\text{C}$$
$$T^* = \ln(0.398) + 0.0170T \quad \text{if } T > 160^\circ\text{C}$$

$$O^* = \ln(3.28) \quad \text{if } DO < 0.02 \text{ ppm}$$
$$O^* = \ln(70.79) + 0.7853\ln(DO) \quad \text{if } 0.02 \text{ ppm} \le DO \le 0.7 \text{ ppm}$$
$$O^* = \ln(53.5) \quad \text{if } DO > 0.7 \text{ ppm.}$$

The F_{en} model was established based on base metal data and is conservative for weld metal. Environmental effects are not considered for seismic load cycles or at small strain amplitude of 0.042 % or less for carbon and low-alloy steels. A comparison between experimental fatigue life and predicted fatigue life for carbon and low-alloy steel is shown in Figure 34.

Separate experiments have been done by Hirano et al. [32] in order to independently evaluate the model for carbon steel. The test specimens were small hollow cylindrical specimens, which were polished before tests were conducted. The tests were performed under BWR conditions with different strain rates, temperatures, dissolved oxygen levels and flow velocities, and both under constant and changing water flow rate conditions and dissolved oxygen levels. The comparison between the predicted fatigue life and experimental fatigue life showed that the fatigue life was predicted within the factor of three, which is smaller than the scatter of environmental fatigue life.

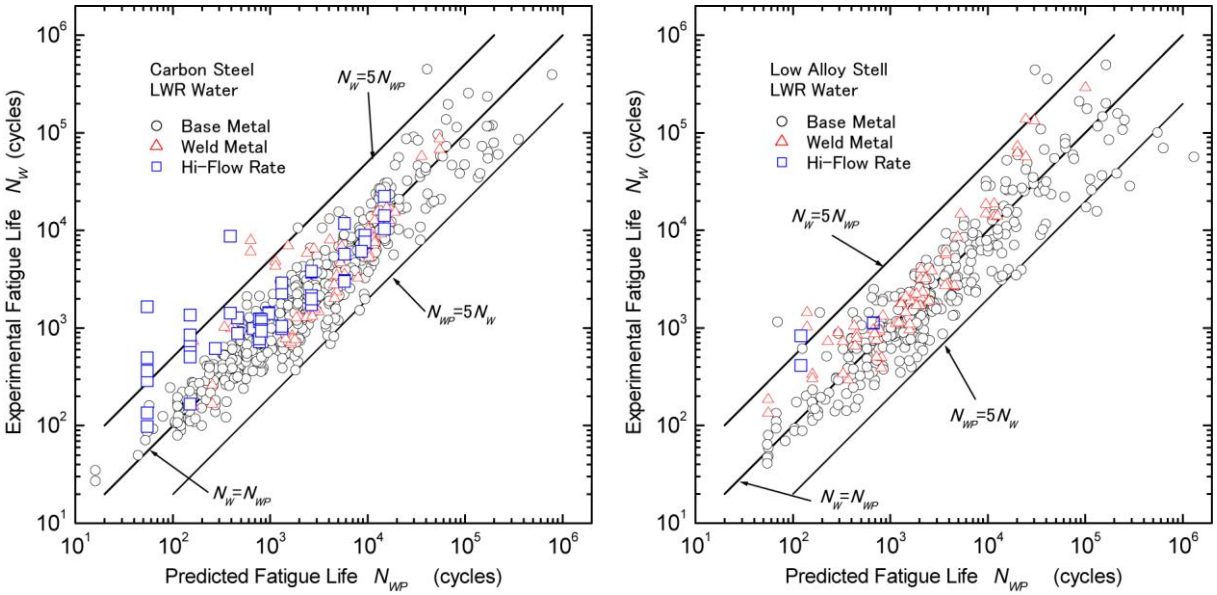

(a) (b)

Figure 34. Comparison of experimental fatigue life to predicted fatigue life for (a) carbon steel and (b) low-alloy steel [47]. The line in the middle indicates when the predicted fatigue life is equal to the experimental fatigue life, and the other two parallel lines correspond to if there is difference by a factor of 5 in either direction.

3.3.1.2 Austenitic stainless steels

For austenitic stainless steel the model [47] is describes as

$$\ln(F_{en}) = (C - \dot{\varepsilon}^*)T^* \tag{5}$$

where C, $\dot{\varepsilon}$ and T are variables that depends on reactor type and are given by the following equations,

$C = 0.992$	for BWR plant
$C = 3.910$	for PWR plant
$\dot{\varepsilon}^* = \ln(2.69)$	for BWR plant if $\dot{\varepsilon}$ > 2.69%/s
$\dot{\varepsilon}^* = \ln(49.9)$	for PWR plant if $\dot{\varepsilon}$ > 49.9%/s
$\dot{\varepsilon}^* = \ln(\dot{\varepsilon})$	for BWR plant if $4 \cdot 10^{-5} \le \dot{\varepsilon} \le 2.69\%/\mathrm{s}$
	and for PWR plant if $4 \cdot 10^{-4} \le \dot{\varepsilon} \le 49.9\%/\mathrm{s}$ (except for Cast SS)
	or $4 \cdot 10^{-5} \le \dot{\varepsilon} \le 49.9\%/\mathrm{s}$ (Cast SS)
$\dot{\varepsilon}^* = \ln(4 \cdot 10^{-5})$	for BWR and PWR plant (Cast SS) if $\dot{\varepsilon} < 4 \cdot 10^{-5}\%/\mathrm{s}$
$\dot{\varepsilon}^* = \ln(4 \cdot 10^{-4})$	for PWR plant (except Cast SS) if $\dot{\varepsilon} < 4 \cdot 10^{-4}\%/\mathrm{s}$
$T^* = 0.000969T$	for BWR plant
$T^* = 0.000782T$	for PWR plant if $T \le 325^\circ\mathrm{C}$
$T^* = 0.254$	for PWR plant if $T > 325^\circ\mathrm{C}$.

This model has the limits that the environmental effects are not considered for seismic load cycles or for small strain amplitude of 0.11 % or less for austenitic stainless steel. A comparison between experimental fatigue life and predicted fatigue life for austenitic stainless steel in BWR and PWR water is shown in Figure 35.

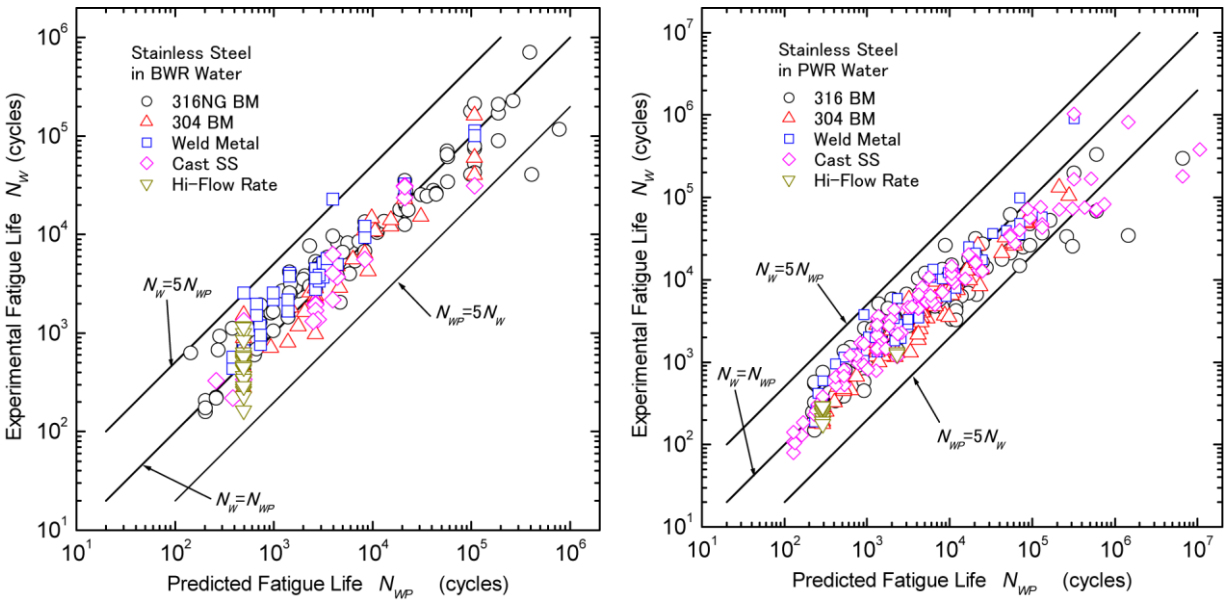

(a) (b)

Figure 35. Comparison of experimental fatigue life to predicted fatigue life for austenitic stainless steel in (a) BWR water and (b) PWR water [47].

3.3.1.3 Nickel-base alloys

JNES has also a model for environmental fatigue life correction factor for nickel-base alloys in BWR and PWR water,

$$\ln(F_{en}) = (C - \dot{\varepsilon}^*)T^* \tag{6}$$

where the parameters C, $\dot{\varepsilon}^*$ and T^* are given by following equations, dependent on the reactor type,

C = -0.112 for BWR plant (Alloy 600)
C = 2.94 for PWR plant (Alloy 600/690)

$\dot{\varepsilon}^* = \ln(0.894)$ for BWR plant if $\dot{\varepsilon}$ > 0.894%/s
$\dot{\varepsilon}^* = \ln(19.0)$ for PWR plant if $\dot{\varepsilon}$ > 19.0%/s
$\dot{\varepsilon}^* = \ln(\dot{\varepsilon})$ for BWR plant if $4\cdot10^{-4} \le \dot{\varepsilon} \le 0.894\%/\mathrm{s}$
and for PWR plant if $4\cdot10^{-4} \le \dot{\varepsilon} \le 19.0\%/\mathrm{s}$
$\dot{\varepsilon}^* = \ln(4\cdot10^{-4})$ for BWR and PWR plant if $\dot{\varepsilon} < 4\cdot10^{-4}\%/\mathrm{s}$

$T^* = 0.000343T$ for BWR plant
$T^* = 0.000397T$ for PWR plant.

For this model environmental effects are not considered for seismic load cycles and for small strain amplitude of 0.11 % or less for nickel-base alloy, as same as that for austenitic stainless steel. A comparison between experimental fatigue life and predicted fatigue life for nickel-base alloys in BWR and PWR water is shown in Figure 36.

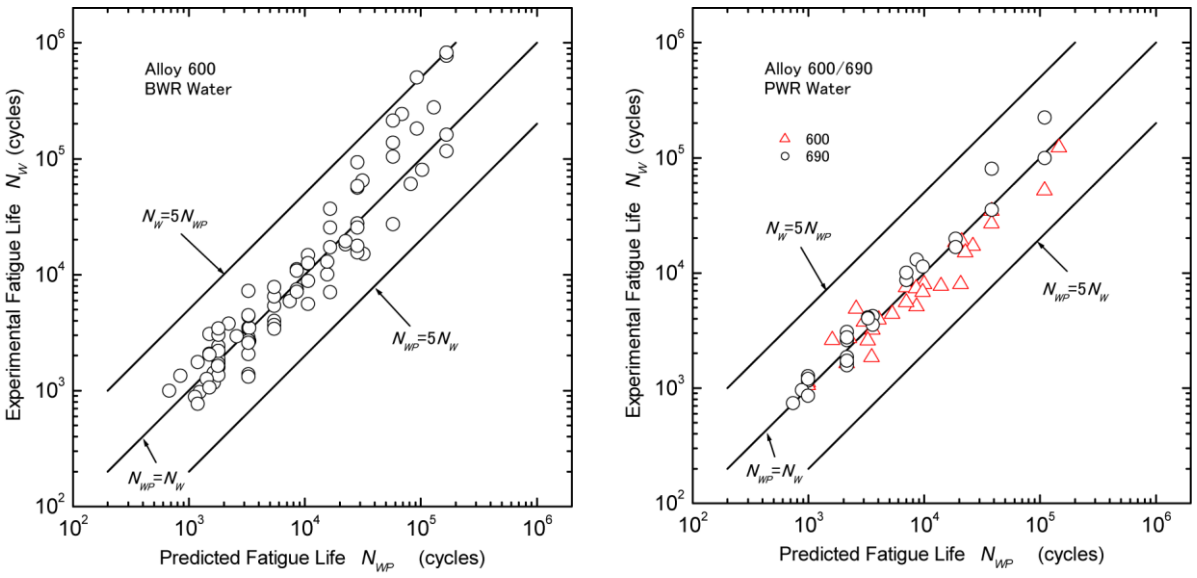

(a) (b)

Figure 36. Comparison of experimental fatigue life to predicted fatigue life for nickel-base alloys in (a) BWR water and (b) PWR water [47].

3.3.2 Model proposed by ANL

The existing fatigue data developed at various establishments and research laboratories worldwide have been compiled by the Pressure Vessel Research Council (PVRC), Working Group on ε-N Curve and Data Analysis. The Argonne National Laboratory (ANL) research [3, 20, 26, 48] is based on an updated version of the PVRC database which includes sources from General Electric Co. [61-64], Japan including Ishikawajima-Harima Heavy Industries (IHI) Co., Mitsubishi Heavy Industries (MHI) Ltd., Hitachi Research Laboratory [21-23, 28-30, 34, 43, 60, 65-78], Argonne National Laboratory [20, 26, 31, 35, 37-39, 48, 79-81], Materials Engineering Associates (MEA) Inc. [82-84], Germany [85, 86], France [87-89] and others [4, 90-95]. The total number of tests in the used database is about 1400, approximately 60% were obtained in water environment ant the remaining in air.

3.3.2.1 Carbon and low-alloy steels

As suggested in the ANL-report NUREG/CR-6909 [3], which presents the latest model developed by ANL, the fatigue life N in LWR environments for carbon and low-alloy steels can be represented by

$$\ln(N) = K_1 - K_2 \ln(\varepsilon_a - K_3) + 0.101 S^* T^* O^* \dot{\varepsilon}^* \quad (7)$$

where the material parameters

$K_1 = 5.951$ for carbon steel
$K_1 = 5.747$ for low-alloy steel

$K_2 = 1.975$ for carbon steel
$K_2 = 1.808$ for low-alloy steel

$K_3 = 0.113$ for carbon steel
$K_3 = 0.151$ for low-alloy steel

and the parameters dependent on dissolved oxygen content in the water, *DO*, the sulphur content in the steel, *S*, the temperature, *T* and the strain rate, $\dot{\varepsilon}$ are defined as

$S^* = 0.015$ if $DO > 1.0$ ppm
$S^* = 0.001$ if $DO \leq 1.0$ ppm and $S \leq 0.001$ wt.%
$S^* = S$ if $DO \leq 1.0$ ppm and $0.001 < S \leq 0.015$ wt.%
$S^* = 0.015$ if $DO \leq 1.0$ ppm and $S > 0.15$ wt.%

$T^* = 0$ if $T \leq 150$°C
$T^* = T - 150$ if 150°C < T < 350°C

$O^* = 0$ if $DO \leq 0.04$ ppm
$O^* = \ln(DO / 0.04)$ if 0.04 ppm < $DO \leq 0.5$ ppm
$O^* = \ln(12.5)$ if $DO > 0.5$ ppm

$\dot{\varepsilon}^* = 0$ if $\dot{\varepsilon} > 1$%/s
$\dot{\varepsilon}^* = \ln(\dot{\varepsilon})$ if $0.001 \leq \dot{\varepsilon} \leq 1$%/s
$\dot{\varepsilon}^* = \ln(0.001)$ if $\dot{\varepsilon} < 0.001$ %/s.

This model is recommended for predicted fatigue lives $\leq 10^6$ cycles. For fatigue lives > 10^6 cycles no model has been presented by ANL, probably in lack of enough experimental data in that area. The nominal environmental fatigue correction factor, $F_{en,nom}$ for carbon and low-alloy steel becomes

$$F_{en,nom} = \exp\left(K_4 - 0.101 S^* T^* O^* \dot{\varepsilon}^*\right) \quad (8)$$

where

$K_4 = 0.632$ for carbon steel

$K_4 = 0.702$ for low-alloy steel.

A threshold strain amplitude is also defined below which LWR coolant environments have no effect on fatigue life, i.e. $F_{\text{en,nom}} = 1$. The threshold strain amplitude is 0.07% (145 MPa stress amplitude) for carbon and low-alloy steels. A comparison between experimental fatigue life and predicted fatigue life for carbon and low-alloy steel is shown in Figure 37.

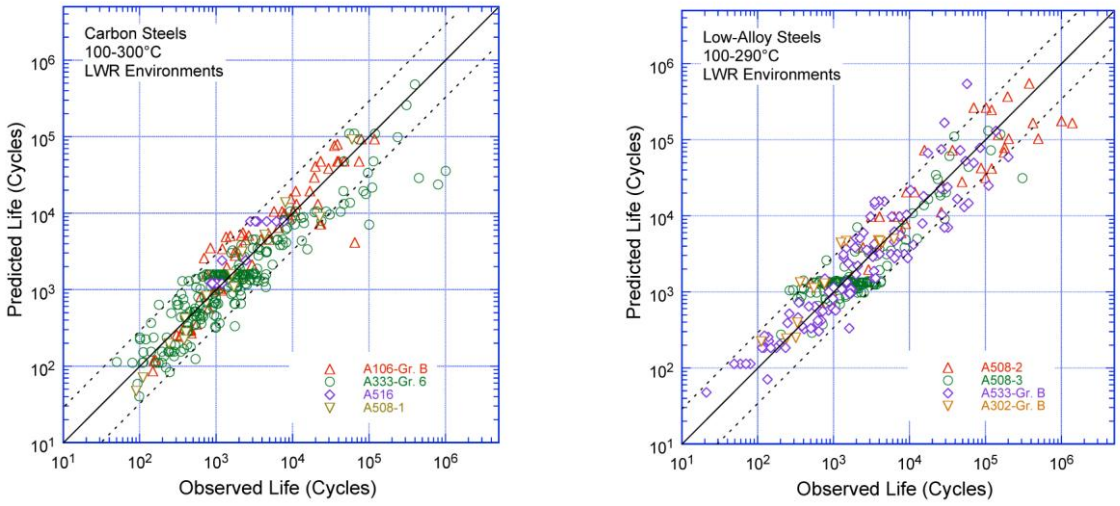

(a) (b)

Figure 37. Comparison of experimental fatigue life to predicted fatigue life for (a) carbon steel and (b) low-alloy steel [3].

3.3.2.2 Austenitic stainless steels

The latest model developed by ANL [3], for the fatigue life of austenitic stainless steels in LWR environments is represented by the equation

$$\ln(N) = C_1 - C_2 \ln(\varepsilon_a - C_3) + T'O'\dot{\varepsilon}' \tag{9}$$

where the material parameters

$K_1 = 6.157$

$K_2 = 1.920$

$K_3 = 0.112$

and T', O' and $\dot{\varepsilon}'$ are transformed temperature, strain rate, and *DO*, defined as

$T' = 0$ if $T \le 150^\circ\text{C}$

$T' = (T - 150)/175$ if $150^\circ\text{C} < T < 325^\circ\text{C}$

$T' = 1$ if $T > 325^\circ\text{C}$

$O' = 0.281$ all *DO* levels

$$\dot{\varepsilon}' = 0 \qquad \text{if } \dot{\varepsilon} > 0.4\ \%/\text{s}$$
$$\dot{\varepsilon}' = \ln(\dot{\varepsilon}/0.4) \qquad \text{if } 0.0004 \le \dot{\varepsilon} \le 0.4\ \%/\text{s}$$
$$\dot{\varepsilon}' = \ln(0.0004/0.4) \qquad \text{if } \dot{\varepsilon} < 0.0004\ \%/\text{s}.$$

This model is recommended for predicted fatigue lives $\le 10^6$ cycles. For fatigue lives $> 10^6$ cycles no model has been presented by ANL, probably in lack of enough experimental data in that area. It should be noted that O' is a constant in this model, and therefore the fatigue life of austenitic stainless steel has no dependence on the dissolved oxygen level. The nominal environmental fatigue correction factor for austenitic stainless steel then becomes

$$F_{\text{en,nom}} = \exp(K_4 - T'O'\dot{\varepsilon}') \qquad (10)$$

where

$$K_4 = 0.734.$$

A threshold strain amplitude is also defined below which LWR coolant environments have no effect on fatigue life, i.e. $F_{\text{en,nom}} = 1$. The threshold strain amplitude is 0.10% (195 MPa stress amplitude). A comparison between experimental fatigue life and predicted fatigue life for austenitic stainless steel is shown in Figure 38.

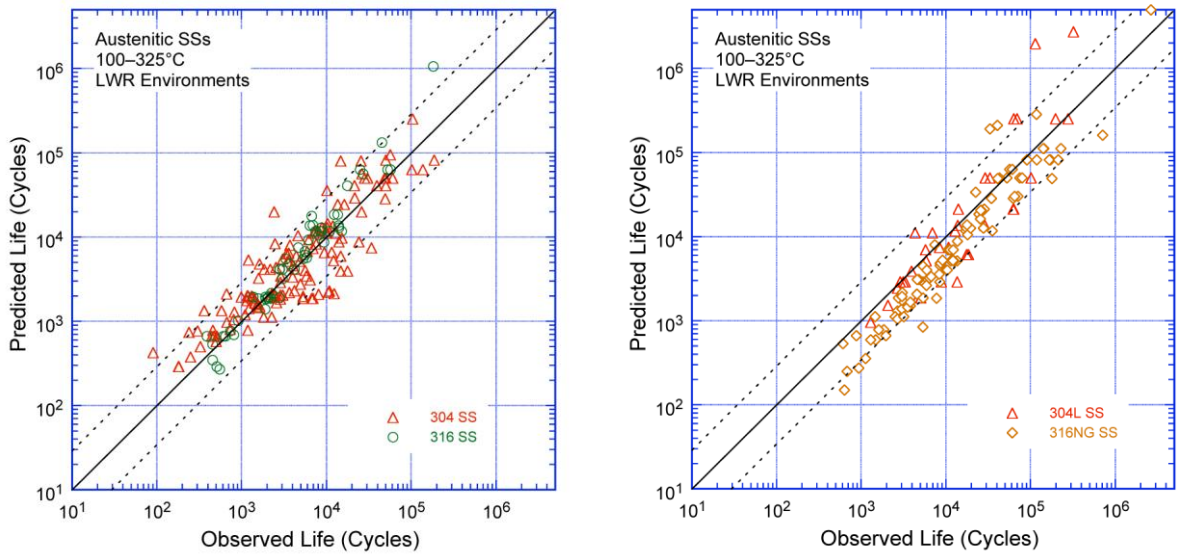

(a) (b)

Figure 38. Comparison of experimental fatigue life to predicted fatigue life for (a) 304 and 316, (b) 304L and 316NG austenitic stainless steel [3].

3.3.2.3 Nickel-base alloys

The existing fatigue data are very limited to develop a fatigue life model for estimating the fatigue life for Ni-Cr-Fe alloys in LWR environments. However environmental effects for these alloys show the same trends as those observed for austenitic stainless steels. ANL has expressed the environmental fatigue correction factor for nickel-base alloys as

$$F_{\text{en,nom}} = \exp(T'O'\dot{\varepsilon}') \qquad (11)$$

where T', O' and $\dot{\varepsilon}'$ are transformed temperature, strain rate, and *DO*, defined as

$$T' = T/325 \quad \text{if } T < 325^{\circ}\text{C}$$
$$T' = 1 \quad \text{if } T \geq 325^{\circ}\text{C}$$

$$O' = 0.09 \quad \text{for NWC BWR water}$$
$$O' = 0.16 \quad \text{for PWR or HWC BWR water}$$

$$\dot{\varepsilon}' = 0 \quad \text{if } \dot{\varepsilon} > 5.0 \text{ \%/s}$$
$$\dot{\varepsilon}' = \ln(\dot{\varepsilon}/5.0) \quad \text{if } 0.0004 \leq \dot{\varepsilon} \leq 5.0 \text{ \%/s}$$
$$\dot{\varepsilon}' = \ln(0.0004/5.0) \quad \text{if } \dot{\varepsilon} < 0.0004 \text{ \%/s.}$$

This model is recommended for predicted fatigue lives ≤ 10^6 cycles. For fatigue lives > 10^6 cycles no model has been presented by ANL, probably in lack of enough experimental data in that area. A threshold strain amplitude has also been defined for Ni-Cr-Fe below which LWR coolant environments have no effect on fatigue life; 0.10% (195 MPa stress amplitude). A comparison between experimental fatigue life and predicted fatigue life for nickel-base alloys in BWR and PWR water is shown in Figure 39.

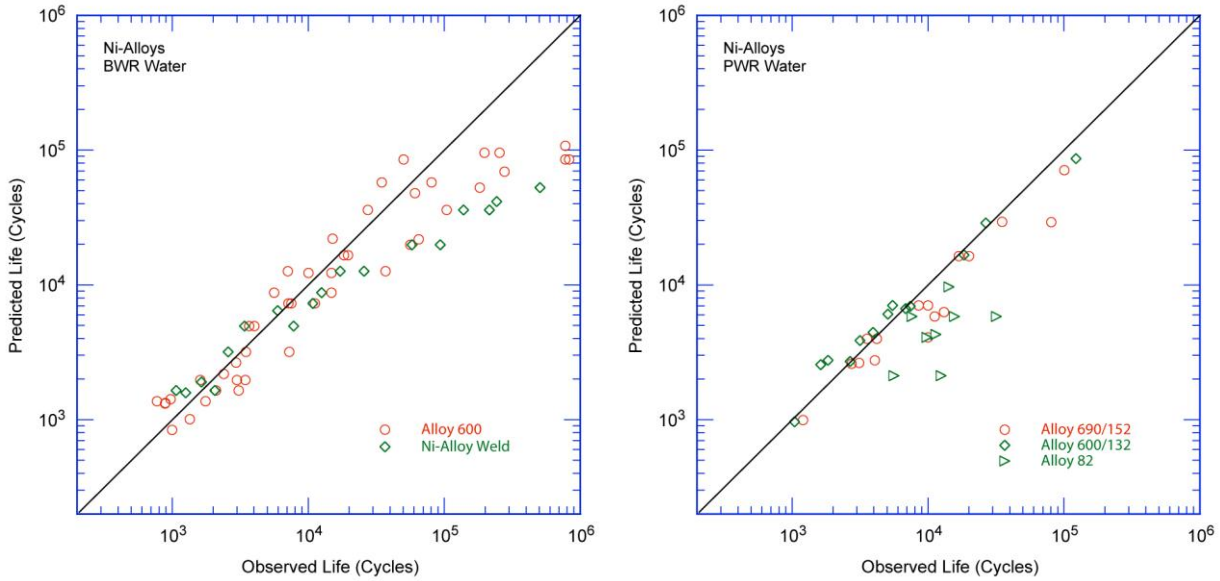

(a) (b)

Figure 39. Comparison of experimental fatigue life to predicted fatigue life for nickel-base alloys in (a) BWR water and (b) PWR water [3].

3.3.3 Calculation of cumulative usage factor

The cumulative fatigue usage factor, U_{en}, considering the effects of reactor coolant environments is calculated as

$$U_{en} = \sum_i U_i F_{en,i} \tag{12}$$

where $F_{en,i}$ is the nominal environmental fatigue correction factor for the *i*th stress cycle (NB-3200) or load set pair (NB-3600) [1]. Because environmental effects on fatigue life occur primarily during the tensile-loading cycle, this calculation is performed only for the tensile stress producing portion of the

stress cycle constituting a load pair. The values of key parameters such as strain rate, temperature, dissolved oxygen in water, and for carbon and low alloy steels sulphur content, are needed to calculate F_{en} for each stress cycle or load set pair [3, 44].

F_{en} can be determined by use of three different methods with varying degrees of complexity and conservatism, the factor multiplication, the simplified and the detailed and method. Any combination of the methods will give conservative results so it is possible to apply these different methods to each section in a stress cycle [44]. In the report by JSME [44] the different methods to determine F_{en} are described, and fatigue evaluation methods for individual components are presented, for example piping and vessels. They have also suggested a method to take reduction in fatigue life due to strain holding into consideration.

3.4 Discussion

For most transients one or several threshold conditions are not satisfied and environmental effects on fatigue are thus moderate. Transients with very strong environmental effects (i.e. with slow stain rates) are usually not very damaging with respect to fatigue damage accumulation because of their small strain amplitudes in combination with the rather limited cycle numbers during the whole lifetime. Thermal transients with large strain amplitudes (e.g. thermal shock), which are very efficient with respect of fatigue damage accumulation per fatigue cycle, are usually related to high strain rates and (very) rare events. Because of the high strain rates, environmental effects do not play a role here. Thermal transients with slow strain rates and strong environmental effects are usually related to small to medium strain amplitudes and infrequent events (e.g. thermal stratification during plant start-up or hot standby. In such cases, in spite of the strong environmental effect, the total accumulated damage is moderate. Transients with large cycle number are usually related to small strain amplitudes and medium to high strain rates (thermal striping or turbulent mixing of cold and hot water in T-joints). But in superposition with thermal stratification and pressurisation and thermal cycles from plant start-up /shut-down, the combination of high cycle number and moderate environmental effects are likely to result in a significant total fatigue damage accumulation [41].

3.4.1 Comparisons between models

The two models have been compared for different LWR environments and materials. Comparisons between the models for carbon steel in BWR and PWR are made in Figure 40 and Figure 41, and in Table 5 and Table 6 are the related F_{en} values presented. In Figure 42 and Figure 43 the comparisons between the models for low-alloy steel in BWR and PWR are presented, together with F_{en} values in Table 7 and Table 8. The austenitic stainless steel comparisons for BWR and PWR are presented in Figure 44 with F_{en} values in Table 9. The BWR environment is here characterised by DO = 0.8 ppm and T = 289˚C, while PWR environment is characterised by DO = 0.1 ppm and T = 325˚C. The results show that the JSME models are in these cases always more conservative or almost the same as the ANL model. The difference between the models is largest for slow strain rates where the JSME, especially for the smaller S value in BWR water, are more conservative. At the most the difference is a factor 7.8, for carbon steel. The models give most equal results for austenitic stainless steel, with a factor 1-2.3 between the F_{en} values.

Overall, there are no significant differences between the JSME and ANL models since most of the database utilized by ANL was provided by Japan [44] and the two models show a similar dependence on the different environmental parameters. Detailed differences between the models are presented below in Table 10. There are some conclusions that can be drawn when comparing these models.

- The ANL model uses separate equations for carbon and low-alloy steels while the Japanese model uses identical equations for these materials.
- There are minor differences in curve fitting for the four major effects (strain rate, sulphur content, temperature and oxygen concentration) between the ANL and JSME models.

- The JSME model specifies different equations for stainless steel in PWR and BWR environments while the ANL model uses identical equations.
- The ANL model applies its own design fatigue curve.
- The JSME model is constructed in a way that when the material and environmental parameters reaches the threshold values, i.e. the values below or above the environment has negligible effect on the fatigue curve, $F_{en} = 1$. This criterion is not set on the ANL model.

A comparison between the models has also been performed by Higuchi [96], also including a comparison to experimental data. An earlier comparison between ANL model and JSME model has also been performed [97]. Some conclusions that have been drawn are

- In comparison with test data the ANL model was not always conservative in PWR water [96] and all lines were not conservative for slow strain rate for carbon and low-alloy steel as well as for stainless steels.
- A better agreement can be seen between the JSME line and the test data [96] regarding temperature dependence for carbon and low-alloy steels.
- In the temperature range 50 to 150˚C are the F_{en}-values from the JSME model about three times higher than the from the ANL model for carbon and low-alloy steels. The ANL line is not conservative at lower temperatures compared to all test data. However, the F_{en} is essentially not large at low temperature ant thus the influence of this difference is not significant.
- The difference between the JSME and ANL estimated temperature dependence for austenitic stainless steels are observed at low temperature but the difference is small because F_{en} is essentially small.
- The JSME estimated temperature dependence for austenitic stainless steel is not the best fit curve to experimental data but serves to connect; i.e., $F_{en} = 1$ at $T = 0$ [47].
- The ANL model is not always conservative at low-DO levels compared to test data for carbon and low-alloy steels [96].
- The ANL model for carbon and low-alloy steels is not conservative against all test sulphur content data except around 0.015% [96].

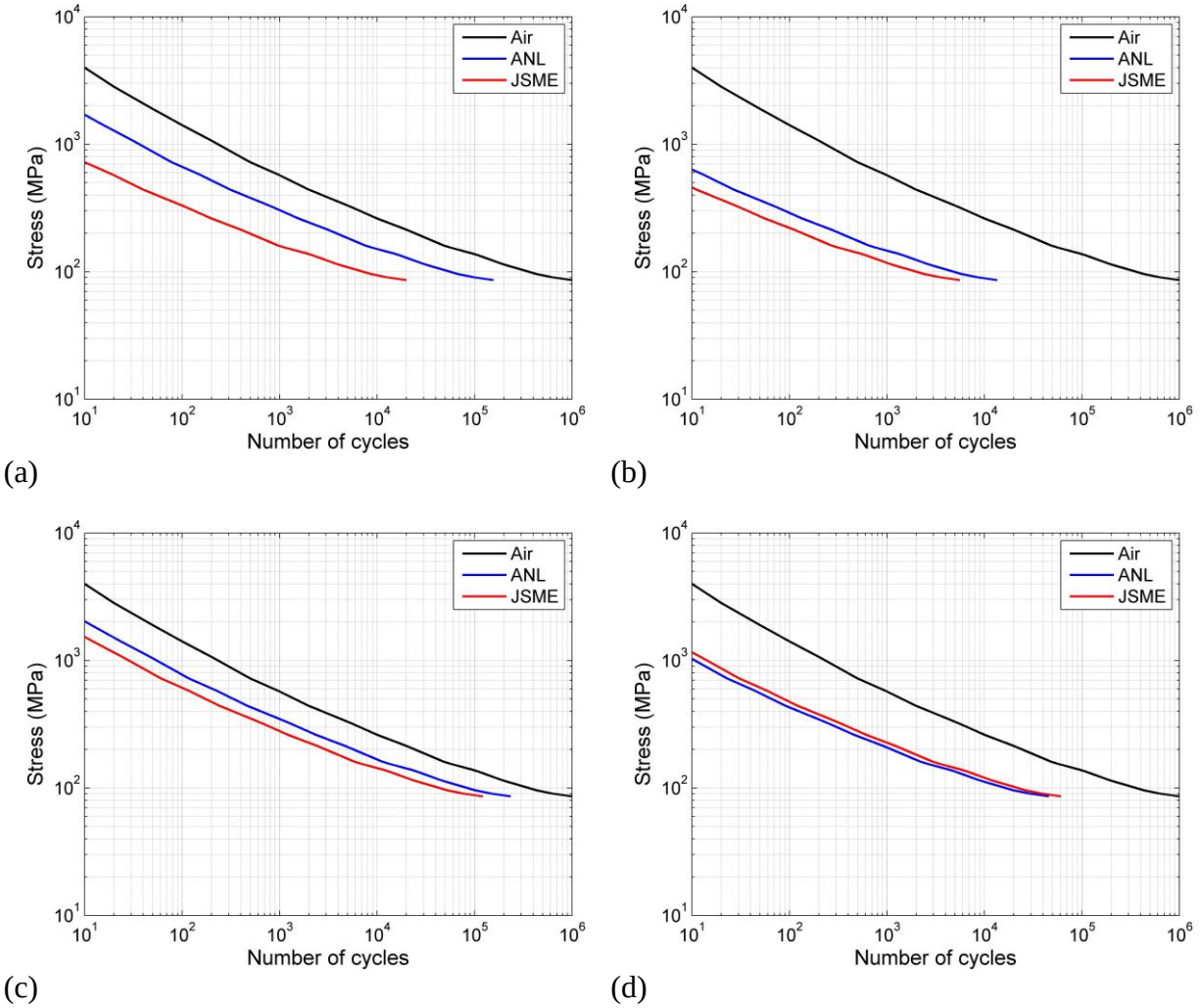

Figure 40. Comparison between estimated fatigue curves from the ANL model and JSME model in BWR environment for carbon steel with (a) $\dot{\varepsilon}$ = 0.0001 %/s, S = 0.005 wt.%, (b) $\dot{\varepsilon}$ = 0.0001 %/s, S = 0.015wt.%, (c) $\dot{\varepsilon}$ = 0.01 %/s, S = 0.005 wt.%, (d) $\dot{\varepsilon}$ = 0.01 %/s, S = 0.015 wt.%.

Table 5. Comparison between calculated F_{en} values for carbon steel in BWR water.

Strain rate, $\dot{\varepsilon}$ (%/s)	Sulphur content, S (wt.%)	F_{en}^{JSME} (JSME model)	F_{en}^{ANL} (ANL model)	$\frac{F_{en}^{JSME}}{F_{en}^{ANL}}$
≤ 0.00004	0.005	50.0	6.40	7.8
≤ 0.00004	0.015	179	74.2	2.4
0.01	0.005	8.22	4.26	1.9
0.01	0.015	16.4	21.8	0.75

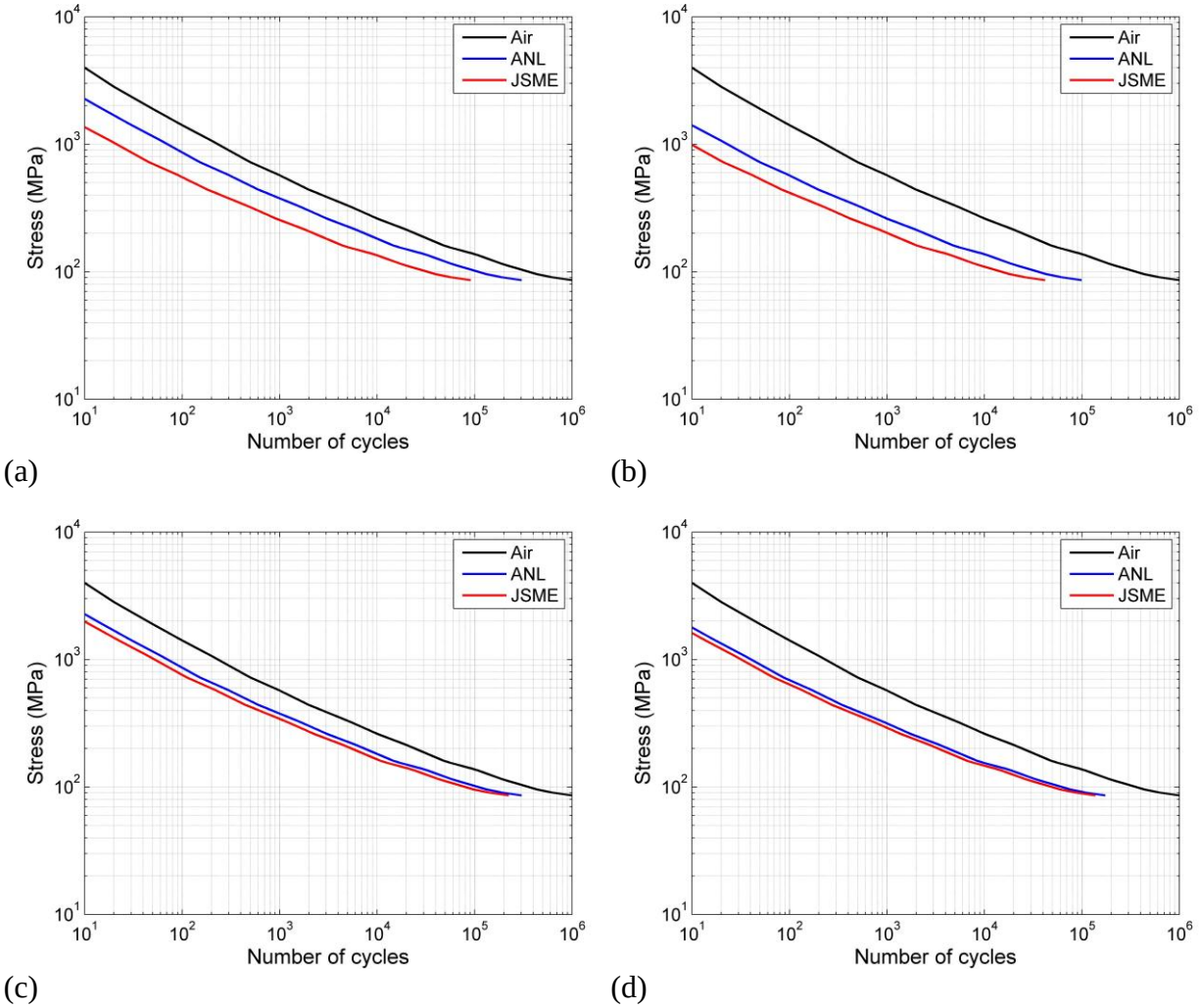

Figure 41. Comparison between estimated fatigue curves from the ANL model and JSME model in PWR environment for carbon steel with (a) $\dot{\varepsilon}$ = 0.0001 %/s, S = 0.005 wt.%, (b) $\dot{\varepsilon}$ = 0.0001 %/s, S = 0.015wt.%, (c) $\dot{\varepsilon}$ = 0.01 %/s, S = 0.005 wt.%, (d) $\dot{\varepsilon}$ = 0.01 %/s, S = 0.015 wt.%.

Table 6. Comparison between calculated F_{en} values for carbon steel in PWR water.

Strain rate, $\dot{\varepsilon}$ (%/s)	Sulphur content, S (wt.%)	F_{en}^{JSME} (JSME model)	F_{en}^{ANL} (ANL model)	$\frac{F_{en}^{JSME}}{F_{en}^{ANL}}$
≤ 0.00004	0.005	10.9	3.29	3.3
≤ 0.00004	0.015	23.9	10.1	2.4
0.01	0.005	4.47	3.29	1.4
0.01	0.015	7.28	5.76	1.3

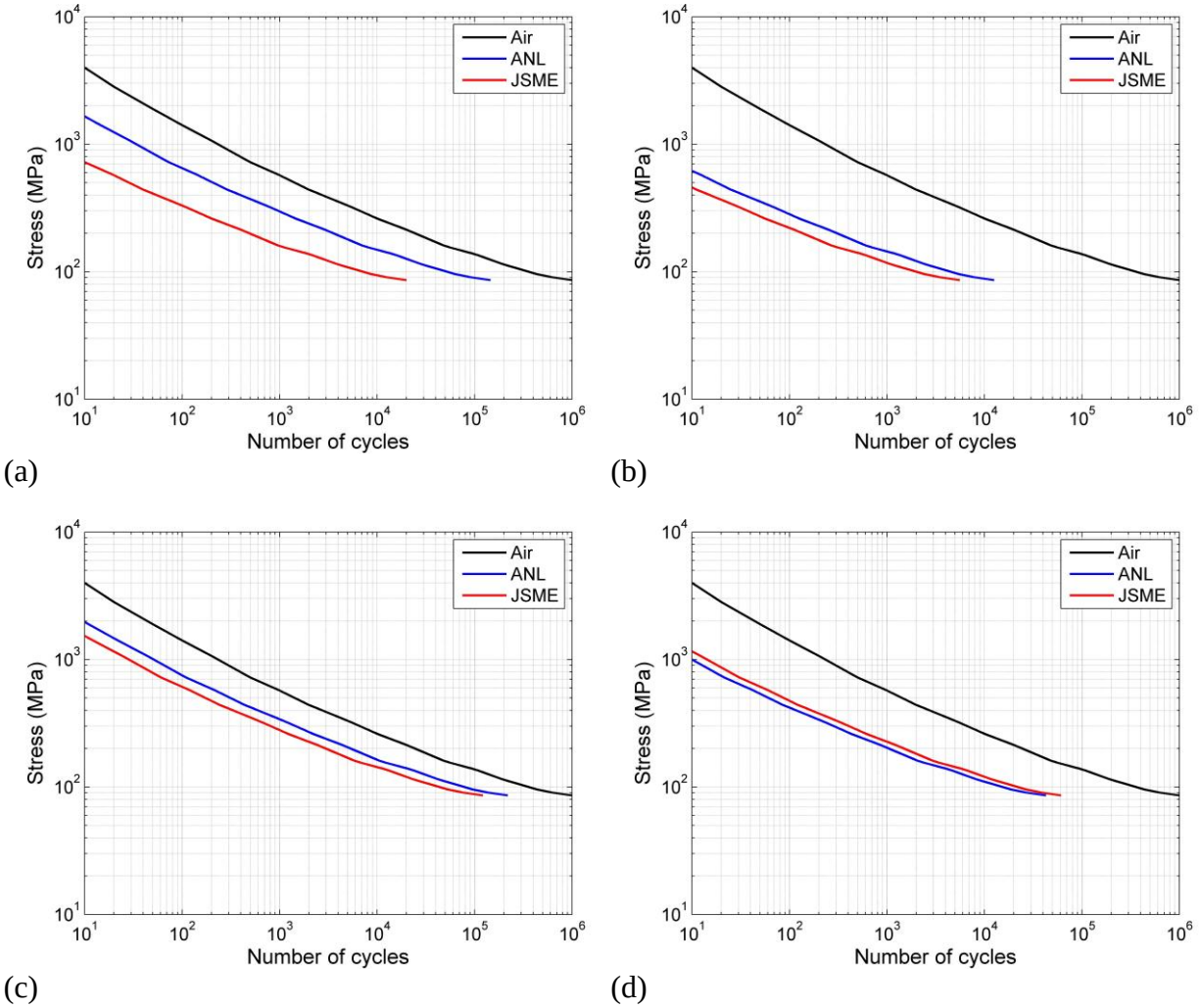

Figure 42. Comparison between estimated fatigue curves from the ANL model and JSME model in BWR environment for low-alloy steel with (a) $\dot{\varepsilon}$ = 0.0001 %/s, S = 0.005 wt.%, (b) $\dot{\varepsilon}$ = 0.0001 %/s, S = 0.015wt.%, (c) $\dot{\varepsilon}$ = 0.01 %/s, S = 0.005 wt.%, (d) $\dot{\varepsilon}$ = 0.01 %/s, S = 0.015 wt.%.

Table 7. Comparison between calculated F_{en} values for low-alloy steel in BWR water.

Strain rate, $\dot{\varepsilon}$ (%/s)	Sulphur content, S (wt.%)	F_{en}^{JSME} (JSME model)	F_{en}^{ANL} (ANL model)	$\frac{F_{en}^{JSME}}{F_{en}^{ANL}}$
≤ 0.00004	0.005	50.0	6.87	7.3
≤ 0.00004	0.015	179	79.5	2.3
0.01	0.005	8.22	4.57	1.8
0.01	0.015	16.4	23.4	0.70

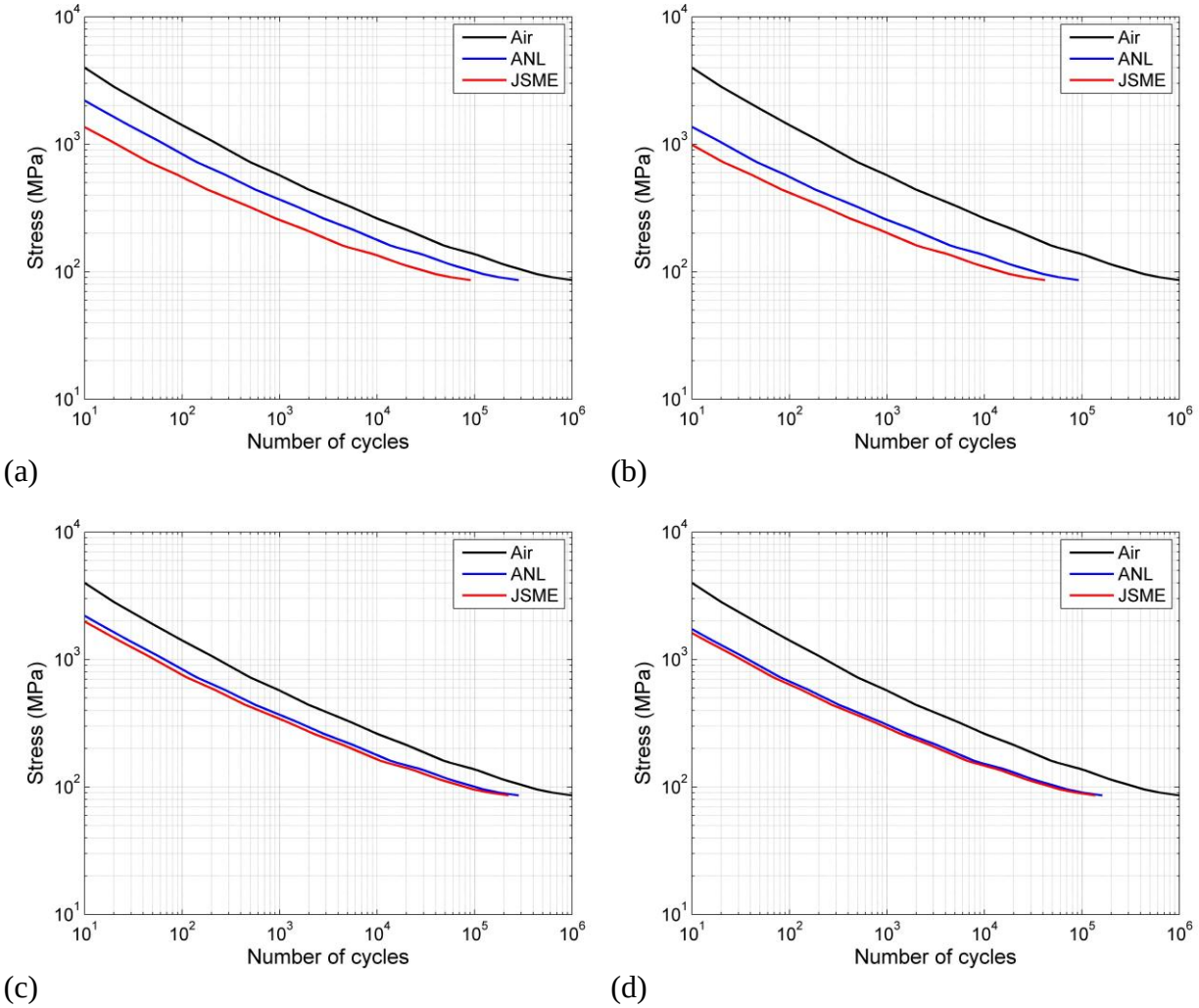

Figure 43. Comparison between estimated fatigue curves from the ANL model and JSME model in PWR environment for low-alloy steel with (a) $\dot{\varepsilon}$ = 0.0001 %/s, S = 0.005 wt.%, (b) $\dot{\varepsilon}$ = 0.0001 %/s, S = 0.015wt.%, (c) $\dot{\varepsilon}$ = 0.01 %/s, S = 0.005 wt.%, (d) $\dot{\varepsilon}$ = 0.01 %/s, S = 0.015 wt.%.

Table 8. Comparison between calculated F_{en} values for low-alloy steel in PWR water.

Strain rate, $\dot{\varepsilon}$ (%/s)	Sulphur content, S (wt.%)	F_{en}^{JSME} (JSME model)	F_{en}^{ANL} (ANL model)	$\frac{F_{en}^{JSME}}{F_{en}^{ANL}}$
≤ 0.00004	0.005	10.9	3.53	3.1
≤ 0.00004	0.015	23.9	10.8	2.2
0.01	0.005	4.47	3.53	1.3
0.01	0.015	7.28	6.18	1.2

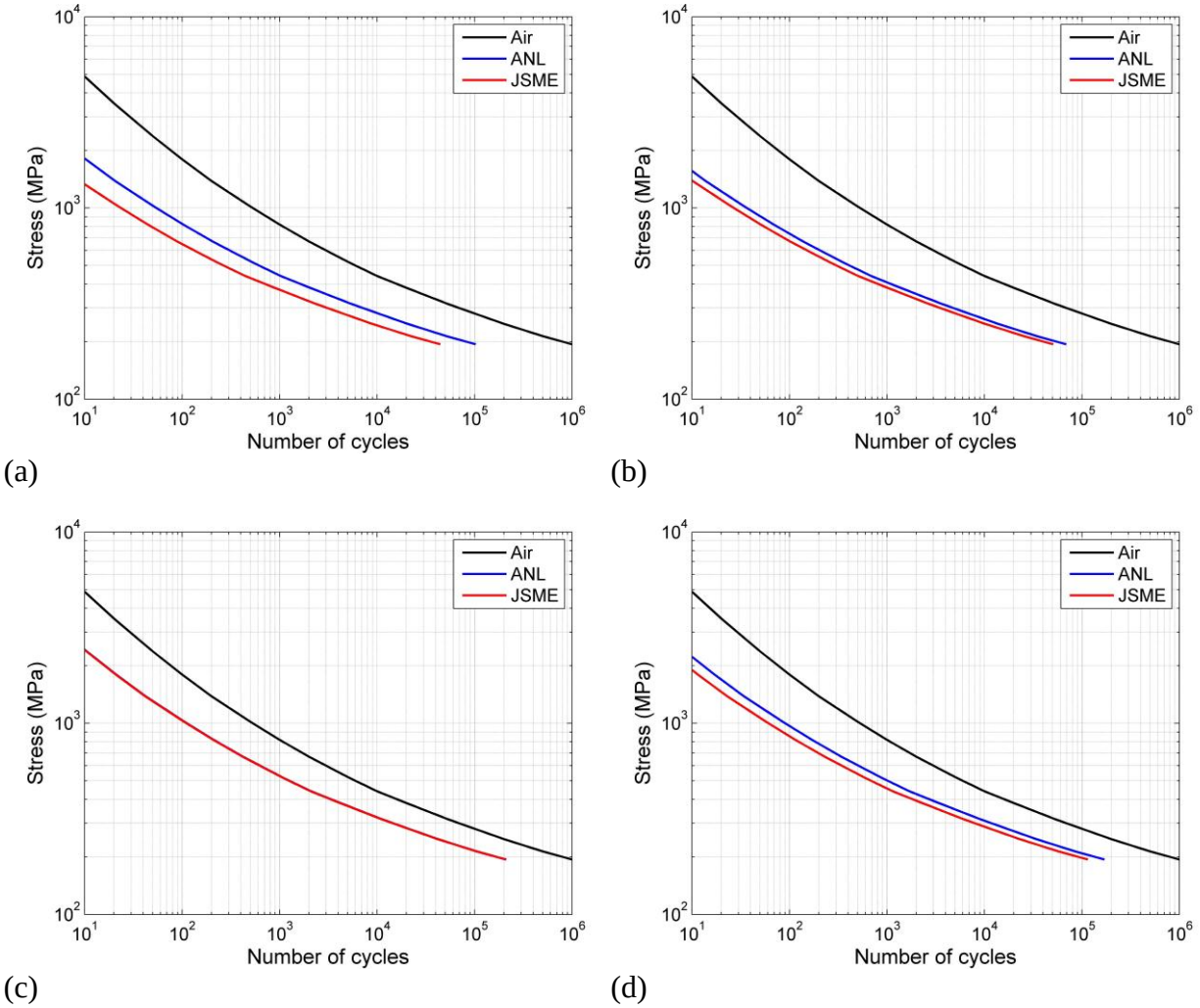

Figure 44. Comparison between estimated fatigue curves from the ANL model and JSME model for austenitic stainless steel in (a) BWR environment with $\dot{\varepsilon}$ = 0.0001 %/s, (b) PWR environment with $\dot{\varepsilon}$ = 0.0001 %/s, (c) BWR environment with $\dot{\varepsilon}$ = 0.01 %/s, (d) PWR environment with $\dot{\varepsilon}$ = 0.01 %/s. Note that the ANL curve and the JSME curve are almost identical in (c) which explains why it is hard to see the blue ANL curve.

Table 9. Comparison between calculated F_{en} values for austenitic stainless steel.

Environment	Strain rate, $\dot{\varepsilon}$ (%/s)	F_{en}^{JSME} (JSME model)	F_{en}^{ANL} (ANL model)	$\frac{F_{en}^{JSME}}{F_{en}^{ANL}}$
BWR	≤ 0.00004	22.5	9.74	2.3
PWR	≤ 0.00004	19.7	14.5	1.4
BWR	0.01	4.79	4.75	1.0
PWR	0.01	8.71	5.87	1.5

Table 10. Detailed differences between the JSME and ANL models dependent on parameter and material.

Parameter	*Material*	*JSME*	*ANL*
Threshold on strain amplitude	carbon and low-alloy steel	0.042%	0.07%
Threshold on strain amplitude	austenitic stainless steel	0.11%	0.10%
Threshold for slow strain rate	carbon and low-alloy steel	0.0001 %/s (if $DO > 0.7$ ppm) or 0.0004 %/s (if $DO \leq 0.7$ ppm)	0.001 %/s
Threshold for slow strain rate	austenitic stainless steel	0.0004%/s (cast stainless steel 0.00004%/s)	0.0004%/s
Threshold for fast strain rate	carbon and low-alloy steel	2.16 %/s ($F_{en} = 1.0$)	1%/s ($F_{en} = 1.88$ for CS and 2.02 for LAS)
Threshold for fast strain rate	austenitic stainless steel	2.69 %/s for BWR, 49.9 %/s for PWR ($F_{en} = 1.0$)	0.4%/s ($F_{en} = 2.08$)
Temperature	carbon and low-alloy steel	F_{en} increases exponentially above 160˚C. F_{en} is independent of temperature in the range from 50 to 160˚C. F_{en} increases exponentially below 50˚C.	F_{en} increases exponentially above 150˚C. F_{en} is independent of temperature under 150˚C.
Temperature	austenitic stainless steel	F_{en} increases exponentially up to 350˚C.	F_{en} increases exponentially above 150˚C and is independent of temperature below 150˚C.
Transition for dissolved oxygen	carbon and low-alloy steel	0.02-0.7 ppm	0.04-0.5 ppm
Sulphur content	carbon and low-alloy steel	F_{en} increases exponentially with increasing sulphur content without threshold	F_{en} increases exponentially but has a threshold at 0.015% and are saturated above

4 CONCLUSIONS

In this report a new proposal for fatigue evaluation of nuclear plant components has been evaluated. This proposal regards an update of fatigue curves and the correction for environmental effects. Some conclusions have been drawn during the study on both areas, see below.

Fatigue curves:

- ANL in USA has performed a unique review of fatigue data. On basis of this review, ANL has proposed new fatigue design curves for austenitic steels, carbon steels and low-alloy steels. The proposals are based on comprehensive studies of data from several modern databases. The data has been consistently evaluated.
- The current ASME III fatigue design curves are based on data from the sixties, the so called Langer data.
- The by far most significant difference between the Langer data and the ANL data holds for austenitic steels in the high cycle fatigue regime.
- For austenitic steels in the high cycle regime ($>10^4$ cycles), the Langer data are higher than the vast majority of data obtained during the past 30 years. Hence the current ASME III fatigue design curves for austenitic steels potentially contain smaller margins than previously expected.
- The ANL design curves are much more consistent with modern data for common austenitic steels, such as SS304/316 than the current ASME III design curves.
- However, the differences between the ANL- design curves for austenitic steels and the corresponding current ASME III curves are quite small in the low cycle regime ($<10^4$ cycles) and hence there is little need for concern about the margins for this region.
- The ANL design curve for carbon steels and low-alloy steels are slightly less conservative than the current ASME III curve. This relaxation of conservatism is consistently motivated by the fatigue data analysed by ANL.
- The ANL design curve for austenitic steels also applies consistently for material type Alloy 600 and Alloy 182.
- Only the fatigue design curves are changed with the ANL proposal. The ASME procedure in itself remains unchanged.
- A distinct feature of the fatigue design procedure in ASME is that small specimen data, loaded in constant amplitude strain control, are used for the design of real components, where the fatigue process may be governed by different parameters. This problem is not at all addressed with the introduction of the ANL fatigue design curves.
- The uncertainty with regards to the transferability of small specimen data is large and the availability of verifying component tests is scarce, in contrast to other modern codes which have been extensively evaluated against data from more realistic specimens. This uncertainty is particularly large for austenitic steels, which are characterized by significant cyclic plastic deformation even for very long fatigue lives.
- It is recommended that future efforts are devoted to investigating the real margins in the ASME III fatigue design procedure by comparing with component test data.

Environmental effects:

- An extensive amount of literature on environmental effects on fatigue has been studied. There is no doubt that LWR environment may significantly decrease the fatigue life in comparison to air environment.
- The experiments on environmental fatigue conducted mainly in Japan and USA are consistent with each other except for small differences.
- The process for the influence of the environment is different for carbon and low-alloy steels as compared to austenitic stainless steels. For carbon and low-alloy steels the environmental effect involves a slip oxidation/dissolution mechanism, whereas the process for austenitic steels most probably involves hydrogen cracking.
- The environmental effects noticed in these recent experiments were not explicitly included in the current design curves. Hence, there is a concern that the margins in the current ASME fatigue design procedure are smaller than expected.
- Applicable models for incorporating environmental effects in fatigue design calculations have been proposed in USA (ANL) and Japan (JSME). These models seem to incorporate the very complex phenomenon of environmental effects in a reasonable way. Presently, no alternative procedures have been developed.
- The controlling parameters in these models are temperature and strain rate, in addition, for carbon and low-alloy steels, the sulphur content in the steel as well as the dissolved oxygen content in the water.
- If the JSME and ANL models are compared, the difference between the models is largest for slow strain rates, especially in BWR water. The JSME model is, in most cases, more conservative.
- There is no obvious reason, on physical grounds, for preferring one model instead of the other.
- The decrease in fatigue life is caused primarily during growth of micro-structurally short cracks. Environmental effects decreases as the cracks grow larger (> 200 μm). Hence, cracks in the fracture mechanical sense should be less sensitive to environmental effects.

5 REFERENCES

1. 2007 ASME Boiler & Pressure Vessel Code, ASME III Division 1, NB-3000, 2007.

2. Cooper, W. E. 1992. The Initial Scope and Intent of the Section III Fatigue Design procedure, Welding Research Council, Inc., Technical Information from a Workshop on Cyclic Life and Environmental Effects in Nuclear Applications, Clearwater, Florida, January 20–21, 1992.

3. Chopra, O.K. and Schack, W. J., 2007. Effect of LWR coolant environments on the fatigue life of reactor materials, NUREG/CR-6909, ANL-06/08.

4. Jaske, C. E., and O'Donnell, W. J., 1977.Fatigue design criteria for pressure vessel alloys, Transactions of the ASME Journal of Pressure Vessel Technology 99, 584–592.

5. Eeten,van P. and Nilsson, F., 2006. Constant and Variable Amplitude Cyclic Plasticity in 316L Stainless Steel, Journal of Testing and Evaluation, 34 (4), 298-311.

6. EN 13445-3, Unfired pressure vessels, Design, 2002.

7. Marquis, G. B., 1995. High cycle spectrum fatigue of welded components, VTT Publications 240.

8. Maddox, S. J., 2001. Fatigue design review task 5 - assembly o favailable fatigue data relevant to pressure equipment design, TWI REPORT NO: 12337/2/01.

9. Solin. J., Nagel, G., and Mayinger, W., 2009. Fatigue curve and stress strain response for stainless steel, SMIRT 20 - Division 1, paper 3135.

10. Jiang, Y., 2008. Benchmark experiments and characteristic cyclic plasticity deformation, International Journal of Plasticity, 24, 1481–1515.

11. IIW, Fatigue design of welded joints and components, Abington Publishing, Cambridge, 1996.

12

13. EN 1993-1-9 Eurocode 3: Design of steel structures - Part 1-9:Fatigue, 2009.

14. Grandemange, J. M., Héliot, J., Le Duff, J.A. , Heng, C., Keim, E., Fricke, S., Smith, N.G., Bate, S.K., Marquis, G., Rahka, K., Zanaboni, P., Cuerto-Felgueroso, C. and Hübel, H., 1998. Reevaluation of fatigue analysis criteria, Framatome Report EE/S 98.317.

15. NRC IE Bulletin No. 79-13 rev. 2. Cracking in feedwater system piping, U.S. Nuclear Regulatory Commission, Washington DC, October 16 1979.

16. NRC Information Notice 93-20. Thermal fatigue cracking of feedwater piping to steam generators, U.S. Nuclear Regulatory Commission, Washington DC, Marsh 24 1993.

17. Hickling, J. and Blind, D., 1986. Strain-induced corrosion cracking of low-alloy steels in LWR systems – Case histories and identification of conditions leading to susceptibility, Nuclear Engineering and Design, 91, 305-330.

18. Iida, K., 1992. A review of fatigue failures in LWR plants in Japan. Nuclear Engineering and Design, 138, 297-312.

19. Kussmaul, K., Blind, D. and Jansky, J., 1984. Formation and growth of cracking in feed water pipes and RPV nozzles, Nuclear Engineering and Design, 81, 105-119.

20. Chopra, O. K., and Shack, W. J. 1998. Effects of LWR coolant environments on fatigue design curves of carbon and low–alloy steels, NUREG/CR–6583, ANL–97/18.

21. Higuchi, M. and Iida, K., 1991. Fatigue strength correction factors for carbon and low-alloy steels in oxygen-containing high-temperature water, Nuclear Engineering and Design 129, 293-306.

22. Hirano, A., Yamamoto, M., Sakaguchi, K., Shoji, T. and Iida, K., 2002. Effects of water flow rate on fatigue life of ferritic and austenitic steels in simulated LWR environment, Pressure Vessel and Piping Codes and Standards – 2002, PVP Vol. 439, Rana, M. D. (ed.), American Society of Mechanical Engineers, New York, PVP2002-1231, 143–150.

23. Hirano, A., Yamamoto, M., Sakaguchi, K. and Shoji, T., 2004. Effects of water flow rate on fatigue life of carbon and stainless steels in simulated LWR environment, Pressure Vessel and Piping Codes and Standards – 2004, PVP Vol. 480, American Society of Mechanical Engineers, New York, PVP2004-2680, 109–119.

24. Hirano, A., Yamamoto, M., Sakaguchi, K., Shoji, T. and Iida, K., 2003. Effects of water flow rate on fatigue life of carbon steel in simulated LWR environment under low strain rate conditions, Transactions of the ASME, 125, 52-58.

25. Hirano, A., Sakaguchi, K. and Shoji, T., 2007. Effects of water flow rate on fatigue life of structural steels under simulated BWR environment, ASME PVP-2007-26423.

26. Chopra, O. K. and Shack, W. J., 2003. Review of the margins for ASME code design curves – effects of surface roughness and material variability, NUREG/CR–6815, ANL–02/39.

27. Higuchi, M. and Sakamoto, H., 1985. Low cycle fatigue of carbon steel in high temperature pure water, in Japanese, Journal of Iron and Steel Institute of Japan, 71, 101-107.

28. Higuchi, M., Iida, K. and Asada, Y., 1995. Effects of strain rate change on fatigue life of carbon steel in high–temperature water, Fatigue and crack growth: environmental effects, modelling studies, and design considerations, PVP Vol. 306, Yukawa, S. (ed.), American Society of Mechanical Engineers, New York, 111–116; also Proceeding of Symposium on Effects of the Environment on the Initiation of Crack Growth, ASTM STP 1298, American Society for Testing and Materials, Philadelphia, 216-231, 1997.

29. Nakao, G., Kanasaki, H., Higuchi, M., Iida, K. and Asada Y., 1995. Effects of temperature and dissolved oxygen content on fatigue life of carbon and low–alloy steels in LWR water environment, Fatigue and crack growth: environmental effects, modeling studies, and design considerations, PVP Vol. 306, Yukawa, S. (ed.), American Society of Mechanical Engineers, New York, 123–128.

30. Kanasaki, H., Hayashi, M. Iida, K. and Asada, Y., 1995. Effects of temperature change on fatigue life of carbon steel in high temperature water, Fatigue and crack growth: environmental effects, modeling studies and design considerations, PVP Vol. 306, Yukawa, S. (ed)., American Society of Mechanical Engineers, New York, 117–122.

31. Gavenda, D. J., Luebbers, P. R. and Chopra, O. K., 1997. Crack initiation and crack growth behavior of carbon and low–alloy steels, Fatigue and Fracture 1, Vol. 350, Rahman, S., Yoon, K. K., Bhandari, S., Warke, R.and Bloom, J. M. (eds.), American Society of Mechanical Engineers, New York, 243–255.

32. Hirano, A., Uchisa, K. and Sakaguchi, K., 2007. Method to evaluate fatigue life of carbon steel under simulated synchronously changing BWR condition, Proceedings of PVP2007, 2007 ASME Pressure Vessel and Piping Division Conference, July 22-26, 2007.

33. Higuchi, M., Sakaguchi, K. and Nomura, Y., 2007. Effects of strain holding and continuously changing strain rate on fatigue life reduction of structural materials in simulated LWR water, ASME PVP-2007-26101.

34. Katada, Y., Nagata, N. and Sato, S., 1993. Effect of dissolved oxygen concentration on fatigue crack growth behavior of A533 B steel in high temperature water, ISIJ International. 33 (8), 877–883.

35. Chopra, O. K. and Shack, W. J., 1998. Low–cycle fatigue of piping and pressure vessel steels in LWR environments, Nuclear Engineering and Design 184, 49–76.

36. Higuchi, M., Tsutsumi, K. Hirano, A. and Sakaguchi, K., 2003. A proposal of fatigue life correction factor Fen for austenitic steels in LWR water environments, Journal of Pressure Vessel Technology, 125 (4), 403-410.

37. Chopra, O. K. and Gavenda, D. J., 1998. Effects of LWR coolant environments on fatigue lives of austenitic stainless steels, Journal of Pressure Vessel Technology 120, 116–121.

38. Chopra, O. K., 1999. Effects of LWR coolant environments on fatigue design curves of austenitic stainless steels, NUREG/CR–5704, ANL–98/31.

39. Chopra, O. K., Alexandreanu, B. and Shack, W. J., 2005. Effect of material heat treatment on fatigue crack initiation in austenitic stainless steels in LWR environments, NUREG/CR–6878, ANL–03/35.

40. Seifert, H.P., Ritter, S. and Leber, H, 2010. Corrosion fatigue behavior of austenitic stainless steels under simulated BWR/HWC and PWR conditions, Paul Scherrer Institute, Paper 200435-

41. Seifert, H. P. and Ritter, S, 2009. Part I Corrosion fatigue of austenitic stainless steels under light water reactor conditions.

42. Chopra, O.K. and Shack, W.J., 2004. Effects of LWR coolant environments on fatigue crack initiation in carbon and low-alloy steels and austenitic stainless steels, Proceedings of 3rd International Conference on Fatigue of Reactor Components, Seville Spain, October 3–6, 2004.

43. Higuchi, M., Sakaguchi, K., Hirano, A. and Nomura, Y. Revised and new proposal of environmental fatigue life correction factor (Fen) for carbon and low–alloy steels and nickel alloys in LWR water environments, Proceedings of the 200 ASME Pressure Vessels and Piping Conference, July 23–27, 2006, Vancouver, BC, Canada, paper # PVP 2006–ICPVT–93194.

44. Codes for nuclear power generation facilities – Environmental fatigue evaluation method for nuclear power plants, The Japan Society of Mechanical Engineers, 2009.

45. Environmental fatigue evaluation method for nuclear power generation facilitites, in Japanese, Japan Nuclear Energy Safety Organization, JNES-SS-0701, 2007.

46. Report on verification of material fatigue reliability under commercial nuclear power reactor environment, in Japanese, Japan nuclear Energy Safety organization, 2007.

47. Higuchi, M., Nomura, Y., Sakaguchi, K. and Hirano, A., 2007. Final proposal of environmental fatigue life correction factor factor (Fen) for structural materials in LWR water environment, Proceedings of PVP2007. 2007 ASME Pressure Vessels and Piping Division Conference, 1, 111-122.

48. Chopra, O. K., Mechanisms and Estimation of Fatigue Crack Initiation in Austenitic Stainless Steels in LWR Environments, NUREG/CR–6787, ANL–01/25, Aug. 2002.

49. Ritter, S. and Seifert, H. P., 2009. Corrosion fatigue crack growth behavior of austenitic stainless steels under simulated LWR conditions, 17th International Corrosion Congress, Corrosion Control in the Service of the Society, October 6-10, 2008, Las Vegs, Nevada, USA, Paper no. 2936.

50. Seifert, H. P. and Ritter, S., 2008. Corrosion fatigue crack growth behaviour of low-alloy RPV and piping steels under BWR conditions, Corrosion Science, 50 (7), 1884-1899.

51. Hänninen, H., Törrönen, K., Kemppainen, M. and Salonen, S., 1983. On the mechanisms of environment sensitive cyclic crack growth of nuclear reactor pressure vessel steels, Corrosion Science, 23 (6), 663-679.

52. Roth, A. and Devrient, B., 2010. Environmental effects on fatigue − possible reasons for the apparent mismatch between laboratory test results and operational experience, Fontevraud 7, Contribution of Materials Investigations to Improve the Safety and Performance of LWRs. Paper Reference A031-T05.

53. Leber, H. J., Ritter, S. and Seifert, H.-P., 2010. Corrosion fatigue initiation behaviour of wrought austenitic stainless pipe steels under simulated BWR/HWC and PWR conditions, Fontevraud 7, Contribution of Materials Investigations to Improve the Safety and Performance of LWRs. Paper Reference A082-T03.

54. Ford, F. P., 1993. Prediction of corrosion-fatigue initiation in low-alloy steel and carbon-steel/water systems at 288˚C, Proceedings of Sixth International Symposium on Environmental Degradation of Materials in Nuclear Power Systems – Water Reactors, Gold, R. E. and Simonen, E. P. (eds.), The Minerals, Metals and Materials Society, 9-18.

55. Higuchi, M, 2004. Revised proposal of fatigue life correction factor Fen of carbon and low alloy steels in LWR water environments, Journal of Pressure Vessel Technology, 126 (4), 438-444.

56. Higuchi, M., 1999. Fatigue curves and fatigue design criteria for carbon and low alloy steels in high-temperature water, ASME PVP, 386, 161-169.

57. Report on verification of material fatigue reliability under commercial nuclear power reactor environments, in Japanese, Japan nuclear Energy Safety Organisation, 2005.

58. Report on verification of material fatigue reliability under commercial nuclear power reactor environment, in Japanese, Japan nuclear Energy Safety Organization, 2006.

59. Sakaguchi, K., Higuchi, M., Hirano, A. and Nomura, Y., 2007. Final proposal of environmental fatigue life correction factor (Fen) for structural materials in LWR water environments, ASME PVP-2007-26100.

60. JNUFAD Database established by Higuchi, M., for structural materials at nuclear power plants, Ishikawajima-Harima Heavy Industries Co., Japan.

61. Hale, D.A., Wilson, S.A., Kiss, E. and Gianuzzi, A.J., 1977. Low-cycle fatigue evaluation of primary piping materials in a BWR environment, GEAP-20244, U.S. Nuclear Regulatory Commission.

62. Hale, D.A., Wilson, S.A., Kass, J.N. and Kiss, E., 1981. Low cycle fatigue behaviour of commercial piping materials in a BWR environment, Journal of Engineering and Material Technology, 103, 15-25.

63. Ranganath, S., Kass, J.N. and Heald, J.D., 1982. Fatigue behavior of carbon steel components in high-temperature water environments, BWR environmental cracking margins for carbon steel piping, EPRI NP-2406, Appendix 3, Electric Power Research Institute.

64. Ranganath, S., Kass, J.N. and Heald, J.D., 1982. Fatigue behavior of carbon steel components in high-temperature water environments, Low-cycle fatigue and life prediction, ASTM STP 770, Amzallag, C., Leis, B.N. and Rabbe, P. (eds), American Society for Testing and Materials, Philadelphia, 436-459.

65. Nagata, N., Sato, S. and Katada, Y., 1991. Low-cycle fatigue behavior of pressure vessel steels in high-temperature pressurized water, ISIJ International 31 (1), 106-114.

66. Higuchi, M., Iida, K. and Sakaguchi, K., 2001. Effects of strain rate fluctuation and strain holding on fatigue life reduction for LWR structural steels in simulated PWR water, Pressure Vessel and Piping Codes and Standards, PVP Vol. 419, Rana, M. D. (ed.), American Society of Mechanical Engineers, New York, 143–152.

67. Fujiwara, M., Endo, T. and Kanasaki, H., 1986. Strain rate effects on the low–cycle fatigue strength of 304 stainless steel in high–temperature water environment. fatigue life: Analysis and prediction, Proceedings of International Conference and Exposition on Fatigue, Corrosion Cracking, Fracture Mechanics, and Failure Analysis, ASM, Metals Park, OH, 309–313.

68. Mimaki, H., Kanasaki, H., Suzuki, I., Koyama, M., Akiyama, M., Okubo, T. and Mishima, Y., 1996. Material aging research program for PWR plants, Aging management through maintenance management, PVP Vol. 332, Kisisel, I. T. (ed.), American Society of Mechanical Engineers, New York, 97–105.

69. Kanasaki, H., Umehara, R., Mizuta, H. and Suyama, T., 1997. Fatigue lives of stainless steels in PWR primary water, Transaction of the 14th International Conference on Structural Mechanics in Reactor Technology (SMiRT 14), Lyon, France, 473–483.

70. Kanasaki, H., Umehara, R., Mizuta, H. and Suyama, T., 1997. Effects of strain rate and temperature change on the fatigue life of stainless steel in PWR primary water, Transaction of the 14th International Conference on Structural Mechanics in Reactor Technology (SMiRT 14), Lyon, France, 485–493.

71. Higuchi, M., and Iida, K., 1997. Reduction in low–cycle fatigue life of austenitic stainless steels in high–temperature water, Pressure Vessel and Piping Codes and Standards, PVP Vol. 353, Jones, D. P.B., Newton, R., O'Donnell, W. J. Vecchio, R., Antaki, G. A., Bhavani, D., Cofie, N. G. and Hollinger, G. L. (eds.), American Society of Mechanical Engineers, New York, 79–86.

72. Hayashi, M., 1998. Thermal fatigue strength of type 304 stainless steel in simulated BWR environment, Nuclear Engineering and Design 184, 135–144.

73. Hayashi, M., Enomoto, K., Saito, T. and Miyagawa, T., 1998. Development of thermal fatigue testing with BWR water environment and thermal fatigue strength of austenitic stainless steels, Nuclear Engineering and Design 184, 113–122.

74. Tsutsumi, K., Kanasaki, H., Umakoshi, T., Nakamura, T., Urata, S., Mizuta, H. and Nomoto, S., 2000. Fatigue life reduction in PWR water environment for stainless steels, Assessment Methodologies for Preventing Failure: Service Experience and Environmental Considerations, PVP Vol. 410-2, Mohan, R. (ed.), American Society of Mechanical Engineers, New York, 23–34.

75. Tsutsumi, K., Dodo, T., Kanasaki, H., Nomoto, S., Minami, Y. and Nakamura, T. 2001. Fatigue behavior of stainless steel under conditions of changing strain rate in PWR primary water, Pressure Vessel and Piping Codes and Standards, PVP Vol. 419, Rana, M. D. (ed.), American Society of Mechanical Engineers, New York, 135–141.

76. Tsutsumi, K., Higuchi, M., Iida, K. and Yamamoto, Y. 2002. The modified rate approach to evaluate fatigue life under synchronously changing temperature and strain rate in elevated temperature water, Pressure Vessel and Piping Codes and Standards – 2002, PVP Vol. 439, Rana, M. D. (ed.), American Society of Mechanical Engineers, New York, 99–107.

77. Higuchi, M., Hirano, T. and Sakaguchi, K., 2004. Evaluation of fatigue damage on operating plant components in LWR water, Pressure Vessel and Piping Codes and Standards – 2004, PVP Vol. 480, American Society of Mechanical Engineers, New York, 129–138.

78. Nomura, Y., Higuchi, M., Asada, Y. and Sakaguchi, K., 2004. The modified rate approach method to evaluate fatigue life under synchronously changing temperature and strain rate in elevated temperature water in austenitic stainless steels, Pressure Vessel and Piping Codes and Standards – 2004, PVP Vol. 480, American Society of Mechanical Engineers, New York, 99–108.

79. Chopra, O. K. and Shack, W. J., 2001. Environmental effects on fatigue crack initiation in piping and pressure vessel steels, NUREG/CR–6717, ANL–00/27.

80. Chopra, O. K. and Shack, W. J., 1997. Evaluation of effects of LWR coolant environments on fatigue life of carbon and low–alloy steels, Effects of the environment on the initiation of crack growth, ASTM STP 1298, Van Der Sluys, W. A., Piascik, R. S. and Zawierucha, R. (eds.), American Society for Testing and Materials, Philadelphia, 247–266.

81. Chopra, O. K. and Smith, J. L., 1998. Estimation of fatigue strain–life curves for austenitic stainless steels in light water reactor environments, Fatigue, environmental factors, and new materials, PVP Vol. 374, Mehta, H. S., Swindeman, R. W., Todd, J. A., Yukawa, S., Zako, M., Bamford, W. H., Higuchi, M., Jones, E. Nickel, H. and Rahman, S. (eds.), American Society of Mechanical Engineers, New York, pp. 249–259.

82. Terrell, J. B., 1988. Fatigue life characterization of smooth and notched piping steel specimens in 288°C air environments, NUREG/CR–5013, EM–2232 Materials Engineering Associates, Inc., Lanham, MD.

83. Terrell, J. B., 1988. Fatigue strength of smooth and notched specimens of ASME SA 106–B steel in PWR environments, NUREG/CR–5136, MEA–2289, Materials Engineering Associates, Inc., Lanham, MD.

84. Terrell, J. B., 1988. Effect of cyclic frequency on the fatigue life of ASME SA–106–B piping steel in PWR environments, J. Mater. Eng. 10, 193–203.

85. Lenz, E., Wieling, N. and Muenster, H., 1988. Influence of variation of flow rates and temperature on the cyclic crack growth rate under BWR conditions, Environmental degradation of materials in nuclear power systems – Water reactors, The Metallurgical Society, Warrendale, PA.

86. Garud, Y. S., Paterson, S. R. Dooley, R. B, Pathania, R. S. Hickling, J. and Bursik, A. 1997. Corrosion fatigue of water touched pressure retaining components in power plants, EPRI TR–106696,Final Report, Electric Power Research Institute, Palo Alto.

87. Amzallag, C., Rabbe, P., Gallet, G. and Lieurade, H.–P., 1978. Influence des conditions de sollicitation sur le comportement en fatigue oligocyclique d'aciers inoxydables austénitiques, Memoires Scientifiques Revue Metallurgie Mars, 161–173.

88. Solomon, H. D., Amzallag, C., Vallee, A. J. and De Lair, R. E., 2005. Influence of mean stress on the fatigue behavior of 304L SS in air and PWR water, Proceedings of the 2005 ASME Pressure Vessels and Piping Conference, July 17–21, 2005, Denver, CO, paper # PVP2005–71064.

89. Solomon, H. D., Amzallag, C., De Lair, R. E. and Vallee, A. J., 2004. Strain controlled fatigue of type 304L SS in air and PWR water, Proceedings of the Third International. Conference on Fatigue of Reactor Components, Seville, Spain, Oct. 3–6, 2004.

90. Conway, J. B., Stentz, R. H. and Berling, J. T., 1975. Fatigue, tensile, and relaxation behavior of stainless steels, TID–26135, U.S. Atomic Energy Commission, Washington, DC.

91. Keller, D. L., 1977. Progress on LMFBR cladding, structural, and component materials studies during July, 1971 through June, 1972, Final Report, Task 32, Battelle–Columbus Laboratories, BMI–1928.

92. Jacko, R. J., 1983. Fatigue performance of Ni–Cr–Fe alloy 600 under typical PWR steam generator conditions, EPRI NP–2957, Electric Power Research Institute, Palo Alto, CA.

93. Dinerman, A. E., 1960. Cyclic strain fatigue of inconel at 75 to 600°F, KAPL–2084, Knolls Atomic Power Laboratory, Schenectady, NY.

94. Mowbray, D. F., Sokol, G. J. and Savidge, R. E., 1965. Fatigue characteristics of Ni–Cr–Fe alloys with emphasis on pressure–vessel cladding, KAPL–3108, Knolls Atomic Power Laboratory, Schenectady, NY.

95. Van Der Sluys, W. A., Young, B. A. and Doyle, D., 2000. Corrosion fatigue properties on alloy 690 and some nickel–based weld metals, Assessment methodologies for preventing failure: Service experience and environmental considerations, PVP Vol. 410-2, Mohan, R. (ed.), American Society of Mechanical Engineers, New York, 85–91.

96. Higuchi, M., 2008. Comparison of environmental fatigue evaluation methods in LWR water, 2008 ASME Pressure Vessels and Piping Division Conference July 27-31, 2008, Chicago, Illinois, USA, PVP2008-61087.

97. Iida, K., Bannai, T., Higuchi, M. and Tsutsumi, K., 2001. Comparison of japanese MITI guideline and other methods for evaluation of environmental fatigue life reduction, Pressure Vessel and Piping Codes and Standards, PVP, vol. 419, Rana, M. D. (ed), American Society of Mechanical Engineers, New York, 73-82.

2011:04

The Swedish Radiation Safety Authority has a comprehensive responsibility to ensure that society is safe from the effects of radiation. The Authority works to achieve radiation safety in a number of areas: nuclear power, medical care as well as commercial products and services. The Authority also works to achieve protection from natural radiation and to increase the level of radiation safety internationally.

The Swedish Radiation Safety Authority works proactively and preventively to protect people and the environment from the harmful effects of radiation, now and in the future. The Authority issues regulations and supervises compliance, while also supporting research, providing training and information, and issuing advice. Often, activities involving radiation require licences issued by the Authority. The Swedish Radiation Safety Authority maintains emergency preparedness around the clock with the aim of limiting the aftermath of radiation accidents and the unintentional spreading of radioactive substances. The Authority participates in international co-operation in order to promote radiation safety and finances projects aiming to raise the level of radiation safety in certain Eastern European countries.

The Authority reports to the Ministry of the Environment and has around 270 employees with competencies in the fields of engineering, natural and behavioural sciences, law, economics and communications. We have received quality, environmental and working environment certification.

Strålsäkerhetsmyndigheten
Swedish Radiation Safety Authority

SE-171 16 Stockholm
Solna strandväg 96

Tel: +46 8 799 40 00
Fax: +46 8 799 40 10

E-mail: registrator@ssm.se
Web: stralsakerhetsmyndigheten.se